This is the accepted manuscript version of the contribution published as:

Teramoto, E.H., **Vogt, C.**, Martins Baessa, M.P., Polese, L., Soriano, A.U., Chang, H.K., **Richnow, H.H.** (2020):
Dynamics of hydrocarbon mineralization characterized by isotopic analysis at a jet-fuel-contaminated site in subtropical climate
J. Contam. Hydrol. **234** , art. 103684

The publisher's version is available at:

http://dx.doi.org/10.1016/j.jconhyd.2020.103684

Journal Pre-proof

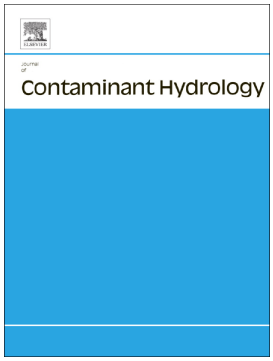

Dynamics of hydrocarbon mineralization characterized by isotopic analysis at a jet-fuel-contaminated site in subtropical climate

Elias H. Teramoto, Carsten Vogt, Marcus P.M. Baessa, Luciana Polese, Adriana U. Soriano, Hung K. Chang, Hans H. Richnow

PII: S0169-7722(20)30273-4

DOI: https://doi.org/10.1016/j.jconhyd.2020.103684

Reference: CONHYD 103684

To appear in: *Journal of Contaminant Hydrology*

Received date: 16 December 2019

Revised date: 24 June 2020

Accepted date: 14 July 2020

Please cite this article as: E.H. Teramoto, C. Vogt, M.P.M. Baessa, et al., Dynamics of hydrocarbon mineralization characterized by isotopic analysis at a jet-fuel-contaminated site in subtropical climate, *Journal of Contaminant Hydrology* (2020), https://doi.org/10.1016/j.jconhyd.2020.103684

This is a PDF file of an article that has undergone enhancements after acceptance, such as the addition of a cover page and metadata, and formatting for readability, but it is not yet the definitive version of record. This version will undergo additional copyediting, typesetting and review before it is published in its final form, but we are providing this version to give early visibility of the article. Please note that, during the production process, errors may be discovered which could affect the content, and all legal disclaimers that apply to the journal pertain.

© 2020 Published by Elsevier.

Journal Pre-proof

DYNAMICS OF HYDROCARBON MINERALIZATION CHARACTERIZED BY ISOTOPIC ANALYSIS AT A JET-FUEL-CONTAMINATED SITE IN SUBTROPICAL CLIMATE

Elias H. Teramoto[1], Carsten Vogt[2], Marcus P.M. Baessa[3], Luciana Polese[1], Adriana U. Soriano[3], Hung K. Chang[1, 4, *], Hans H. Richnow[2]

[1] São Paulo State University, UNESP, Environmental Studies Center (CEA) and Basin Studies Laboratory (LEBAC), Rio Claro, Brazil

[2] Helmholtz Centre for Environmental Research – UFZ, Leipzig, Germany

[3] Petrobras Research Center – CENPES, Rio de Janeiro, Brazil

[4] São Paulo State University, UNESP, Dept. of Applied Geology, Rio Claro, Brazil

*Corresponding author: chang@rc.unesp.br

Journal Pre-proof

DYNAMICS OF HYDROCARBON MINERALIZATION CHARACTERIZED BY ISOTOPIC ANALYSIS AT A JET-FUEL-CONTAMINATED SITE IN SUBTROPICAL CLIMATE

ABSTRACT

Release of benzene, toluene, ethylbenzene, and xylene (BTEX) as components of the light non-aqueous phase liquids (LNAPL) contaminates soil and groundwater. Assessing the mechanisms of degradation and mineralization of BTEX in groundwater helps understand the migration of the dissolved plume, enabling the reduction of risks to humans. Here, we studied the fate of ethylbezene, m,p-xylenes and o-xylenes and the accompanying formation of methane in a Cenozoic lateritic aquifer in Brazil by compound-specific carbon stable isotope analysis (CSIA), to gain insights into the complex dynamics of release and biodegradation of BTEX in the LNAPL source zone. The enrichment of $\partial^{13}C$ in aromatic compounds dissolved in groundwater compared to the corresponding compounds in LNAPL indicate that CSIA can provide valuable information regarding biodegradation. The isotopic analysis of methane provides direct indication of oxidation mediated by aquifer oxygenation. The $\partial^{13}C\text{-}CO_2$ values indicate methanogenesis prevailing at the border and aerobic biodegradation in the center of the LNAPL source zone. Importantly, the isotopic results allowed major improvements in the previously developed conceptual model, supporting the existence of oxic and anoxic environments within the LNAPL source zone.

Journal Pre-proof

Key words: BTEX mineralization, methanogenesis, isotopic analysis, CSIA, interphase mass transfer

1. INTRODUCTION

Hydrocarbon-derived fuels represent an import source of energy worldwide. The accidental release of hydrocarbons because of leakage of storage tanks or pipeline rupture represents a typical situation for groundwater contamination. Whenever that a large volume of petroleum fuel is spilled, it can migrate down the unsaturated zone and reach and saturate zone, forming often a light non-aqueous phase liquids (LNAPLs). In the vadose zone, petroleum is distributed as a non-aqueous phase in the pores of the soil. On the top of the saturated zone LNAPL may fill pores and forming a multiphasic context with oil, gas and water when the water table is fluctuating and may releases soluble compounds (mainly benzene, toluene, ethylbenzene, and xylenes, or BTEX) to the water by interphase mass transfer. Because BTEX compounds released to groundwater are relatively water-soluble and mobile, predicting their fate in the saturated zone is crucial for establishing remediation goals and actions in petroleum-contaminated site management. Under favorable conditions, the degradation of hydrocarbons driven by microbial activity may efficiently limit the spread of BTEX plumes.

The isotopic enrichment of aromatic hydrocarbons related to microbial-mediated breakdown is supported by many field and laboratory studies (Blum et al., 2009; Dorer, Vogt, Neu, Stryhanyuk, & Richnow, 2016; Feisthauer et al., 2012; Mancini et al., 2003; Morasch, Richnow, Schink, Vieth, & Meckenstock,

2002; Schmidt et al., 2004; Vogt et al., 2008). In the last two decades, the technique of compound-specific stable isotope analysis (CSIA) has become a well-established method to quantitatively assess the biodegradation of contaminants such as aromatic hydrocarbons in groundwater (Vogt et al., 2016). This methodology is based on the finding that bacteria-mediated degradation consumes preferentially the molecules with the lighter isotope species (e.g., ^{12}C and ^{1}H), because the activation energy to break covalent-bond-containing light isotopes is lower compared to that of heavier substituents, leading to stable-isotope fractionation of the target molecules. Consequently, CSIA represents a valuable tool to identify and measure the extent of naturally induced contaminant reduction in groundwater (Elsner et al., 2005). Additionally, isotope fractionation may also be induced by some physical process, such as diffusion to vapor phase (Bouchard et al., 2008), transverse dispersion (Rolle et al., 2010), and sorption (Schüth et al., 2003). However, the isotope fractionation due to phase partitioning is small (Kopinke et al. 2017) and, therefore, unlikely to have large effects in the field (Kopinke et al., 2005).

In the LNAPL source zone, entrapped hydrocarbons in the pore system can release soluble compounds over a timescale of decades by interphase mass-transfer processes (Eberhardt and Grathwohl, 2002; Teramoto and Chang, 2017; Thornten et al., 2013). The mass transfer of BTEX from NAPL to groundwater by diffusion does not generate detectable isotopic fractionation (Aeppli et al., 2009; Heße et al., 2014). Under these conditions, CSIA may not offer conclusive evidence of hydrocarbon mineralization, and only a few studies have focused on isotopic characterization dominated by mass-transfer phenomena (Aeppli et al., 2009; Heße et al., 2014).

Journal Pre-proof

Large proportion of BTEX released by mass-transfer is biodegraded within the LNAPL source zone by distinct metabolic pathways. Among them, methanogenesis is known to require more energy than pathways with other electron acceptors from a thermodynamic point of view. However, several reports have demonstrated that hydrocarbons can be mineralized by methanogenesis owing to syntrophic relationships of microbial consortia composed of fermenters and methanogens (Gieg et al., 2014; Lueders, 2017; Morris et al., 2013); this process can become dominant if other energetically more favorable electron acceptors are no longer available. Methanogenesis has been identified as an important, or even dominant, process related to hydrocarbon degradation in subsurface environments (Garg et al., 2017; Jiménez et al., 2016; Ramos et al., 2014; Reinhard et al., 2005; Teramoto and Chang, 2019). Methanogenic degradation of hydrocarbons by a consortium of bacteria and archaea initiates with fermentation reaction causing the hydrocarbons to degrade into acetate and hydrogen in the initial step (Zengler). Methanogens form methane via pathways that are commonly classified based on the type of carbon precursor utilized by them. The primary methanogenic pathways are referred to as: hydrogenotrophic (carbonate reduction), acetotrophic (fermentation), and methylotrophic which is be characterized by the isotope composition of methane (Whiticar, 1999). The investigation on isotopic CH_4 in hydrocarbon-contaminated sites has been conducted by several researchers (Balabane, et al., 1987; Games et al., 1978; Revesz et al., 1995; Whiticar & Faber, 1986). The methanogenesis pathway promotes the enrichment of remaining hydrocarbon, simultaneously producing CH_4 highly depleted in ^{13}C (“isotopically light methane”) and CO_2 highly enriched in ^{13}C

Journal Pre-proof

("isotopically heavy carbon dioxide") (Amos et al., 2011; Conrad et al., 1997; Feisthauer et al., 2011). However, if methane is oxidized by aerobic methanotrophic bacteria, the reaction promotes isotopic enrichment of methane and isotopic depletion of CO_2 along the methane gradient because of the strong stable carbon (and hydrogen) isotope effect on bacterial methane oxidation (Amos et al., 2011; Feisthauer et al., 2011; Revesz et al., 1995; Whiticar and Faber, 1986). In addition, the mineralization of hydrocarbons which are usually depleted in ^{13}C owing to their principally biological origin generates isotopically "light" CO_2 (Conrad et al., 1997; Revesz et al., 1995, Whiticar, 1999). Hence, at sites contaminated by hydrocarbons, the carbon isotope signature of CO_2 can be affected by several different processes: the oxidation of hydrocarbons and methane produces "light" CO_2, whereas methanogenesis produces "heavy" CO_2. Background CO_2 can stem from sediment carbonates, soil respiration, or the atmosphere, adding variable ^{13}C signatures into the pool (Conrad et al., 1997).

The seasonal precipitation pattern at our site lead to large fluctuation of the water table and vertical smearing of the LNAPLs in the sediment column (e.g., Durnford et al., 1991; Steffy et al., 1998). The upward movement of a water table driven by groundwater recharge causes the entrapment of air in the pores in the uppermost portion of the saturated zone (Faybishenko, 1995; Fry et al., 1997; Williams and Oostrom, 2000; Marinas et al., 2013; Mcleod et al., 2015). The entrapped air releases oxygen into the groundwater (Mcleod et al., 2015; Williams & Oostrom, 2000) which may support oxidation processes. The zone containing the pores that are partially filled by entrapped air is known as the "quasi-saturated zone" (Faybishenko, 1995). The air entrapment is

Journal Pre-proof

associated with the presence of “excess air”, that is, the gases (including oxygen) are present at concentrations higher than those required for equilibrium with atmosphere (Holocher et al., 2002). Despite the potential impacts on the biogeochemistry of hydrocarbon biodegradation, thus far, the effects of aquifer oxygenation have not been investigated in detail.

The ability of the CSIA technique to assess the subsurface hydrocarbon biodegradation was demonstrated at numerous sites in temperate climates located in the northern hemisphere. In subtropical and tropical climates, distinct geochemical and hydrological features (for example, elevated groundwater temperature, wide-range fluctuating water table, and abundance of iron in the aquifer sediment) prevail, and studies demonstrating the suitability of the CSIA technique under these conditions are limited. The most prominent characteristic observed in the subtropical and tropical climates is non-aqueous phase entrapment controlled by wide-range water table fluctuation and elevated groundwater temperature, which may cause increased biodegradation kinetics. Because of the lack of studies, the applicability of the isotopic techniques in hydrocarbon-contaminated aquifers in subtropical and tropical environments remain unclear. To address this gap, we aimed to evaluate, for the first time, the suitability of the CSIA technique in a jet-fuel-contaminated site situated in a subtropical climate, by investigating the isotopic composition of BTEX in the aqueous and oil phases. In addition, we performed isotopic analyses of CH_4 and CO_2 in the aqueous phase to trace the fate of CH_4 produced by BTEX biodegradation under methanogenic conditions in the iron-depleted zones.

Journal Pre-proof

2. METHODS

2.1. Site background

2.1.1. Hydrogeology

The study area is located in the municipality of Paulínia, São Paulo, Brazil. The Cenozoic shallow aquifer is composed of clayey sands, coarse sand lenses, sandy clays, and clayey silts (Bordignon et al. 2016; Teramoto and Chang, 2017). The geometry of the channelized sandy bodies and the widespread floodplain facies indicate a typical meandering river depositional environment dominated by flood plains (Teramoto and Chang, 2017). Because hydraulic conductivity is intrinsically related to aquifer lithology, a high variability in hydraulic conductivity is observed. The values of hydraulic conductivities determined by slug tests performed on 64 monitoring wells range between 1.2×10^{-7} and 2.4×10^{-4} m/s, with a geometric mean of 2.8×10^{-5} m/s (Teramoto and Chang, 2017). The average hydraulic gradient is 0.0036 in the northeast region and increases to the southwest, toward the discharge zone, reaching a value of 0.0176. Figure 1 shows the potentiometric map, the inferred limit of the source zone, and the locations of the monitoring and pumping wells in the study area.

Journal Pre-proof

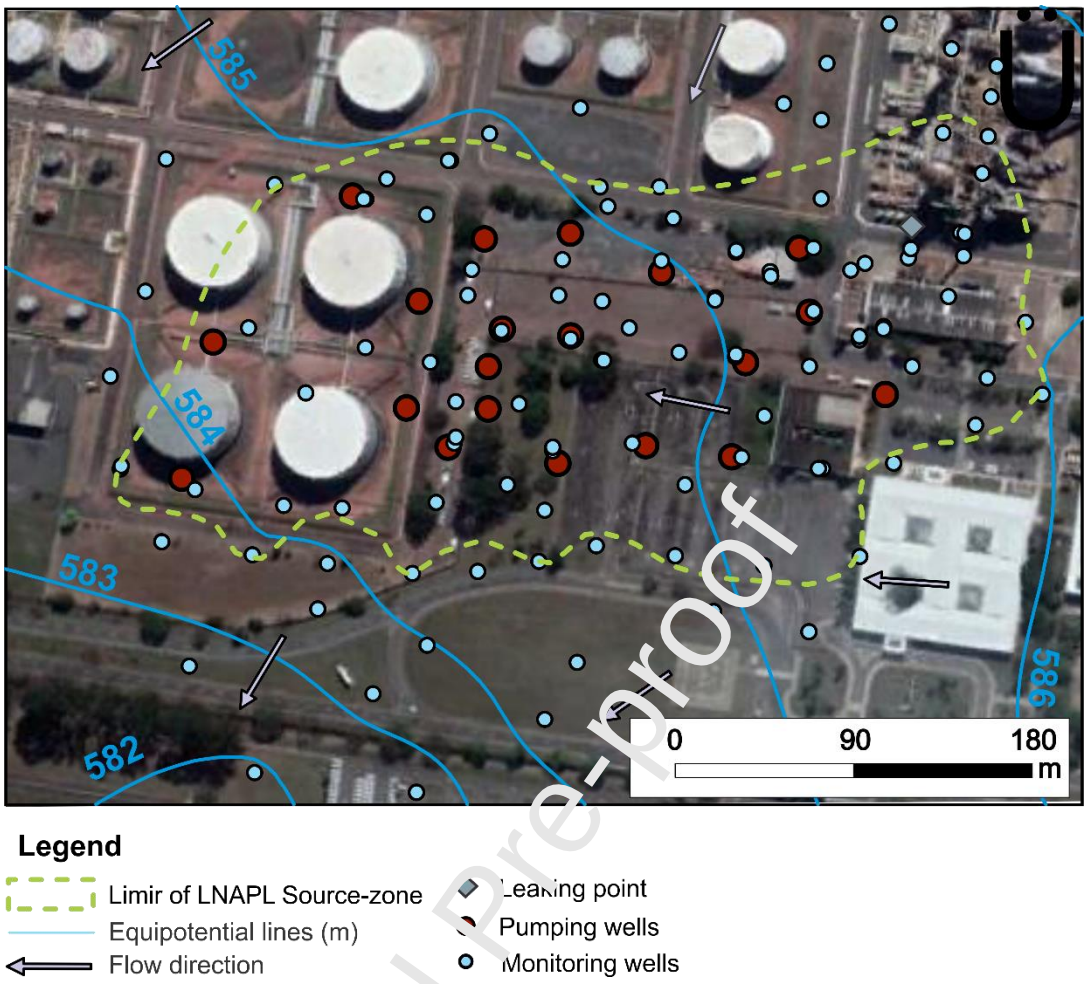

Figure 1 – Location of monitoring and pumping wells in the study area and delineation of the source zone contaminated by LNAPL.

A large quantity of jet fuel is present in the subsurface, with an estimated volume of 520 m^3 (Pede, 2009). The long-term monitoring of water table depth indicates that the water table fluctuates within a range of 3.5 m; the maximum groundwater level is typically reached in May and falls steadily until December (Teramoto and Chang, 2017).

Due to the large annual fluctuation of the water table, most of the monitoring wells were installed within 2 meters of water column and 2 to 3

Journal Pre-proof

meters of unsaturated zone, resulting in filter length of 4 to 5 meters. In order to obtain more specific information from deeper intervals (2 or 3 meters below the water table), multi-level wells with separated 1-meter filter section were installed.

2.1.2. Groundwater Remediation

Since 2005, a pump-and-treat remediation was operated in different modes. Initially, it was operated through four pumping wells. From 2008 to 2009, five additional wells were incorporated into the system. From 2010 to 2011, the remediation was paused and from 2011 to the present, operation resumed with 20 active pumping wells (Figure 1). To determine the limit of LNAPL spread, the plumes of the dissolved BTEX compounds were monitored. A total of 104 monitoring wells were installed in an area of 264,600 m^2. The LNAPL recovery was possible only during the four dry years, when the water table was sufficiently low (Pede, 2009). The volume of water extracted varied between 1.8 to 27 m^3/day. The capture zone during the dry seasons is presented via potentiometric maps (Teramoto and Chang, 2018).

2.1.3. Distribution and solubilization of LNAPL

Because of the large fluctuations of water table (~4 meters along 15 years), the LNAPL forms an entrapped phase below the water table, as demonstrated in a recent investigation using laser-induced fluorescence (Isler et al., 2018). Figure 2 presents the transect SW-NE with 5 Laser Induced

Fluorescence (LIF) tests, 2 of them, previously presented by Isler et al. (2018) (LIF-02 and LIF-05).

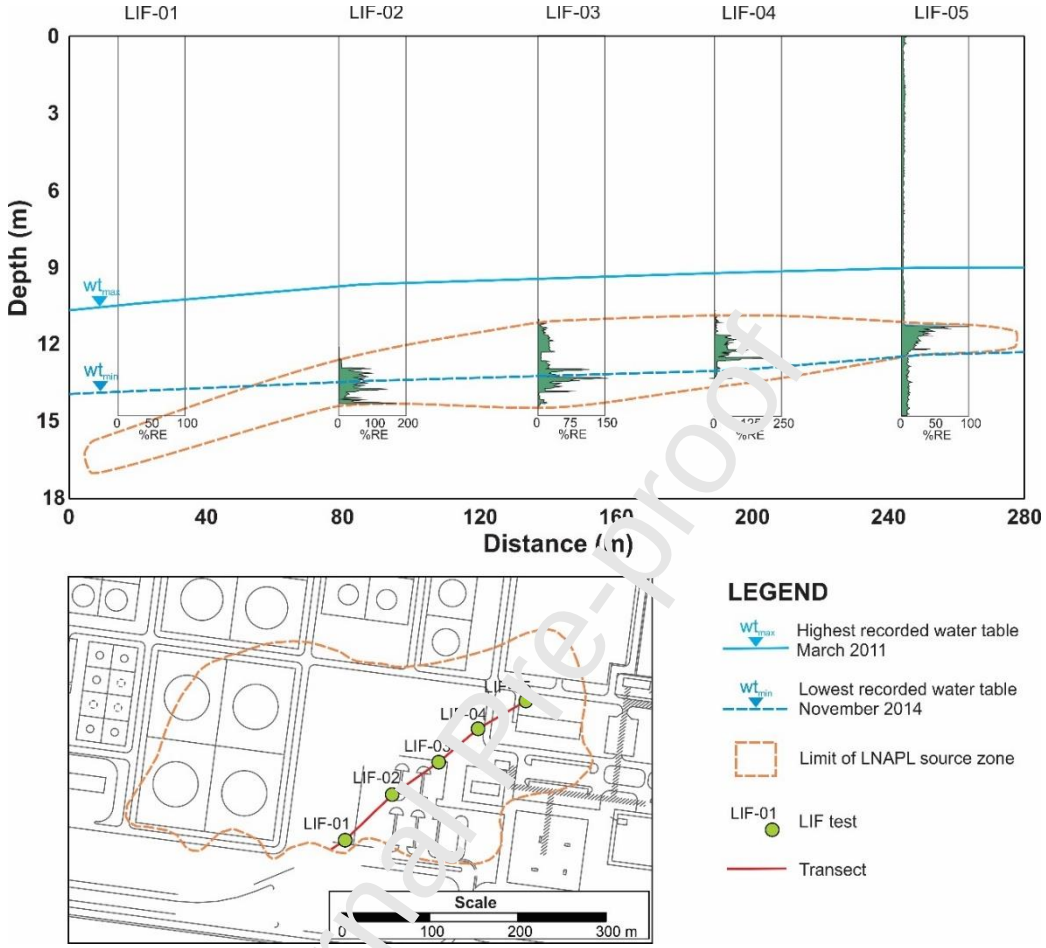

Figure 2 – Transect with LIF investigation showing the vertical delimitation of LNAPL source zone. The lowest and highest level of the recorded water table was found November 2014 and March 2011.

The LIF tests show the upper and lower delimitation of the LNAPL in pore system (Figure 2). Importantly, LIF-01 does not show significant fluorescence until 14.8 m depth, but the sediment samples collected in this point presented oil phase in samples collected during the drilling of monitoring wells.

The BTEX concentration in the aqueous phase reflects the concentration of these compounds in the entrapped LNAPL (Teramoto & Chang, 2017). Because the pores with high non-aqueous saturation deplete slowly, the concentration in regions with high saturation typically exhibits still high concentration in aqueous phase (Teramoto & Chang, 2017).

2.1.4. Dissolved BTEX plume

The high flow velocity should sustain the development of large dissolved plumes in response to the rapid advective movement of the water-soluble compounds in the source zone. However, a noticeable feature of this site is that the narrow plumes of BTEX are developed by advective movement of solubilized BTEX, and each liter of the plume is characterized by the presence of few micrograms. Teramoto and Chang (2019) have suggested that the plume is rather short and relatively stable over time; further, high degradation kinetics contribute to stabilization of the plume, despite its high flow velocity.

Several studies have revealed that the rate of biodegradation of dissolved hydrocarbon increases with an increase in temperature, with upper threshold reaching at approximately 35 °C (e.g., Deeb and Alvarez-Cohen, 1999; Alagappan and Cowan, 2004; Yadav et al., 2012; Zeman et al., 2014). Likely, the solubilization of BTEX plumes is constrained by elevated rates of biodegradation, favored by high groundwater temperature, which is approximately 26 °C at this site (Teramoto and Chang, 2019).

2.1.5. Geochemistry and Microbiology of LNAPL source zone

Journal Pre-proof

Shallow groundwater is an open system buffered by the carbonate system, particularly by high PCO_2 found in the unsaturated zone. Typical values of PCO_2 found in tropical regions range between $10^{-1.8}$ to $10^{-1.4}$ atm (Brook et al., 1983). Bordignon et al. (2015) have shown that the CO_2 concentration in vadose and unsaturated zone is high, reaching over 50,000 ppmv.

Jet fuel is the main electron donor at this filed site, and BTEX compounds are leaching from the LNAPLs and transported by ground water flow because of their higher solubility's than aliphatic hydrocarbons. The seasonal dynamics of this system are a constraint for interpretation of geochemical and isotopic parameters for determination of natural attenuation processes as degradation and dissolution of contaminants are linked to changing conditions. Long-term geochemical monitoring indicates high concentration of both Fe^{2+} and CH_4 (Figure 3), supporting the iron reduction and methanogenesis as main mechanisms driving hydrocarbon mineralization (Teramoto and Chang, 2019).

Journal Pre-proof

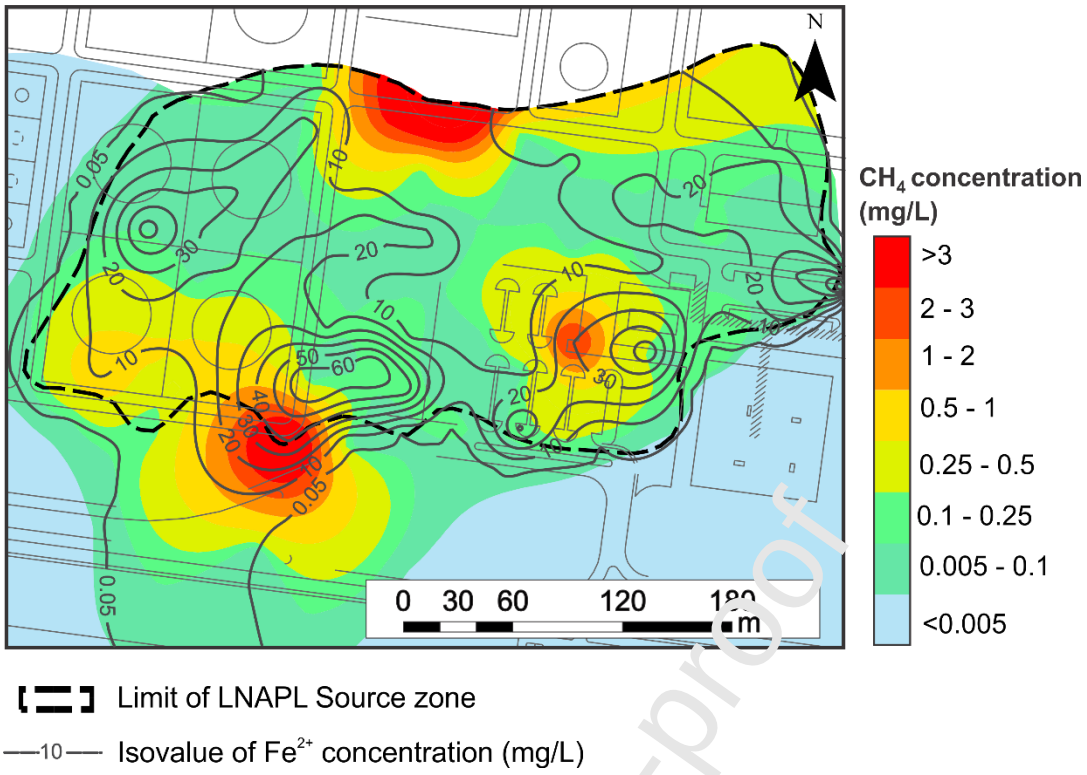

Figure 3 – Map of Fe^{2+} and CH_4 concentration isocontours in May 2012, supporting the occurrence of Fe(III) reduction and methanogenesis as hydrocarbon biodegradation pathways (After Teramoto & Chang, 2019).

2.2. Isotopic analysis

To evaluate the isotopic compositions of aromatic compounds of LNAPL, eight floating oil samples were collected at monitoring wells in December 2014 using disposable bailer. Additionally, one sample of fresh jet fuel was also analyzed. To characterize the isotopic composition of BTEX and methane for both aqueous and oil phases, we conducted three campaigns (March 2015, April 2016, and December 2017) of groundwater sampling (Figure 4). The water samples were analyzed for BTEX compounds only in the first two sampling campaigns (March 2015 and April 2016), and for methane in all three.

Journal Pre-proof

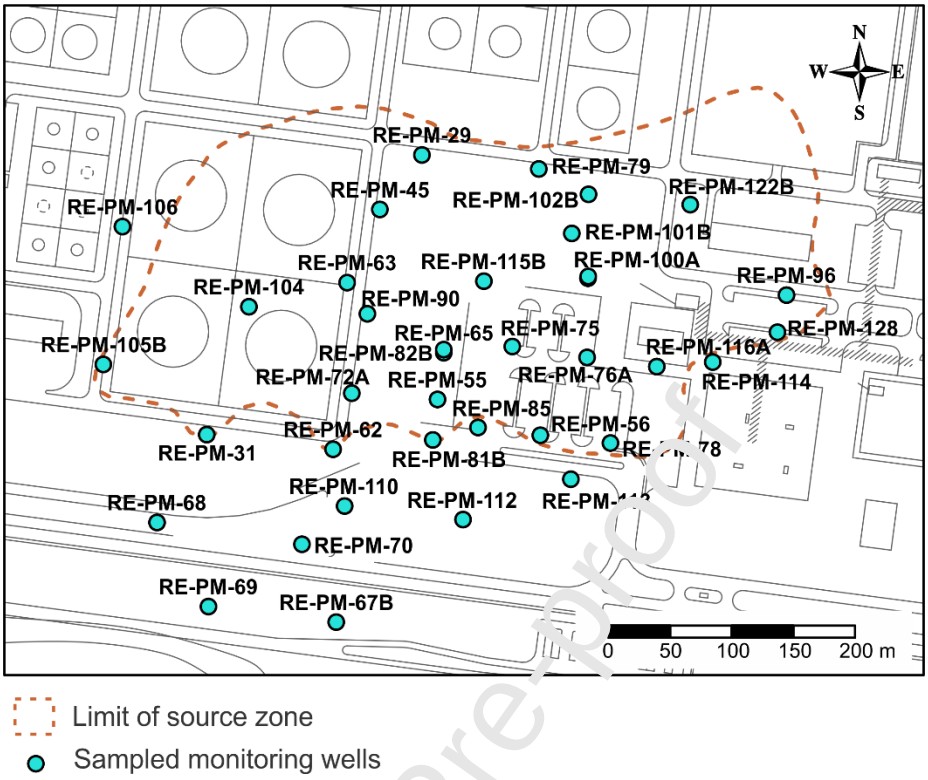

Figure 4 – Distribution of wells sampled for isotopic analysis.

2.2.1. Determination of isotopic signature of BTEX compounds

To address the isotopic characterization of BTEX compounds in the LNAPL source zone, samples of LNAPL and groundwater were collected. The LNAPL samples were collected in the monitoring well during the second quarter of 2014 within the dry season using a disposable bailer. The groundwater samples were collected in two sampling campaigns using low flow methodology (EPA, 1996) in March 2015 and April 2016 during the wet season. In these periods the water table is at its maximum level recorded in these years.

Journal Pre-proof

For isotope analysis of BTEX in the aqueous phase, 1 L Schott bottles were filled with groundwater and NaOH pellets were added (enough to maintain pH > 12) to preserve the samples. Next, in the lab the samples were subjected to extraction with 5 mL of n-pentane for 7 h on a shaker table in a room maintained at 9 °C and were kept to a pH between 10 and 12, following procedures described in the literature (Feisthauer et al., 2012). The n-pentane extracts were analyzed in a gas chromatograph (GC; model 7890A, Agilent Technology) that was coupled to a mass spectrometry system (IRMS; MAT 253, Thermo Fisher Scientific, Germany) and automatic sampler (Combi PAL model, CTC Analytics). The methods for stable isotope analysis was described by (Feisthauer et al., 2012).

The GC was equipped with a ZB-1 column (60 m × 0.32 mm × 1 µm, Zebron) for separation of benzene, toluene, ethylbenzene, and xylene isomers. The initial temperature was set at 40 °C, held constant for 5 min, then increased at 3 °C/min to 90 °C, and finally increased at 20 °C/min to 250 °C where it was held for 3 min. The helium flow was held constant at 2 mL/min and 1.6 mL/min for carbon and hydrogen measurements, respectively. For carbon stable isotope analysis, the BTEX compounds were converted at 980 °C on a CuO/Ni/Pt catalyst to water and carbon dioxide which was subsequently measured by IRMS. For hydrogen isotope analysis, the separated BTEX compounds were transformed at 1440 °C in a ceramic tube (GC-pyrolysis, Thermo Fisher Scientific) into graphite and molecular hydrogen gas which was subsequently analyzed by IRMS.

Journal Pre-proof

The most common expression for stable isotope ratios of a given compound is the deviation d(x) from an international standard. The isotope values are reported as delta notation (δ^{13}C) in units per mil (‰):

$$\delta^{13}[‰] = \frac{R_{sample} - R_{standard}}{R_{standard}} \; x \; 1000 \qquad (1)$$

where R_{sample} is the isotope ratio $^{13}C/^{12}C$ of the sample and $R_{standard}$ is the carbon stable isotope ratio of the standard. As isotope shifts are usually in the per mil range, they are by definition multiplied by a factor of 1000. The carbon and hydrogen isotopic signatures are reported as δ values in parts per thousand (‰) relative to international reference materials, which are Vienna Pee Dee Belemnite (VPDB) for carbon and Standard Mean Ocean Water (SMOW) for hydrogen (Coplen et al., 2006; Coplen, 2011, Schimmelmann et al., 2016).

For both carbon and hydrogen isotope measurements, each sample was analyzed at least three times, the results are reported as the mean in delta notation according to Eq. (1), together with the standard deviation.

Journal Pre-proof

2.3 Quantitative analysis of BTEX

BTEX concentrations were determined in samples extracted with n-pentane for isotope analysis (see 2.2). The n-pentane extracts were analyzed in a gas chromatograph (GC; model 7890A, Agilent Technology) equipped with an autosampler (Combi PAL model, CTC Analytics) and coupled to a mass spectrometer (MS; model 5975C, Agilent). Chromatographic conditions for GC-MS concentration analysis were the same as described for isotopic analysis of BTEX compounds (see 2.2).

2.2.2. Determination of isotopic signature of methane

To determine the $\delta^{13}C$ of dissolved CH_4 and CO_2, approximately 170 mL of groundwater were transferred into 200 mL serum bottles previously amended with approximately 20 g of NaCl (to reduce microbial metabolism and gas solubility, favoring its partitioning to the headspace), and the bottles were immediately closed with butyl rubber stoppers and aluminum crimp seals. Samples were stored upside down at 4 °C until the analysis. Directly before isotopic measurement, the samples were acidified with HCl to reach pH 2, as described in the literature (Fischer et al., 2004). Subsequently, headspace samples of 50 to 100 µL were injected into the GC equipped with a CP-PoraBOND Q column (50 m × 0.32 mm × 0.5 µm, Varian) and separated at a constant temperature of 40 °C and a constant helium flow of 2 mL/min, as described in a recent study (Teramoto and Chang, 2019). Each sample was analyzed at least three times to obtain the mean; the standard deviation of the isotope value was typically better than 0.5%.

Journal Pre-proof

3. RESULTS

3.1. Aqueous concentration of ethylbenzene, m,p-xylenes and o-xylene

During the sample collection for isotopic characterization, the BTEX concentrations were measured in three sampling campaigns (Table 1 of the Supplementary Material) and showed high variability. The BTEX concentrations were measured in March 2015 and April 2016 (Figure 5). Benzene and toluene

were found in much lower concentration than ethylbenzene and xylenes. BTEX concentrations are high in the center of the LNAPL source zone and decrease with the groundwater flow toward the edges. Moreover, BTEX concentrations are higher in wet season (Figure 5a e 5b) than in dry season (Figure 5c) in response to cyclic annual water table fluctuations (Teramoto and Chang, 2017).

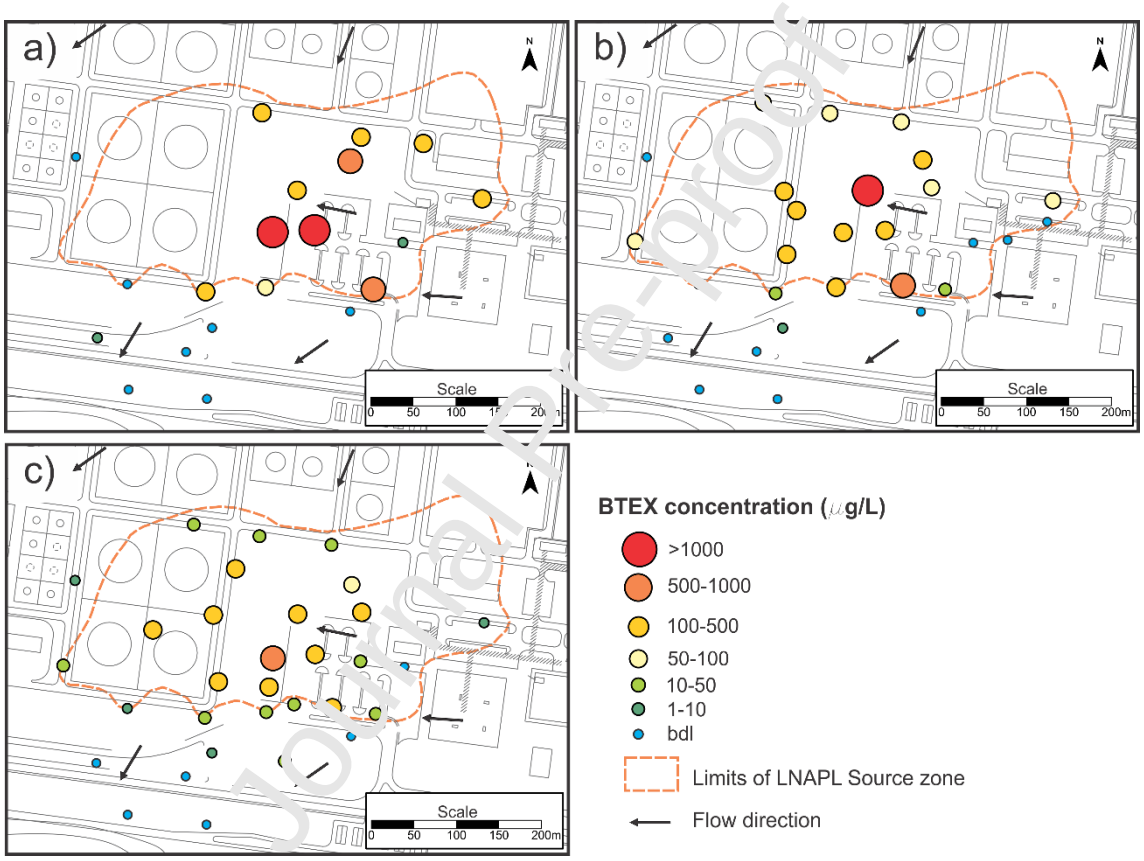

Figure 5 – Distribution of measured BTEX: a) March 2015; b) April 2016; c) December 2017. The concentrations are higher in the center, decreasing toward the border of the LNAPL source zone. bld = below detection limit.

3.2. Isotopic analysis of BTEX within the source zone

To evaluate the initial signature of BTEX compounds released into the aqueous phase, we determined the isotopic signature of BTEX extracted from the oil phase under the assumption that the isotope signature of the residual fraction had not been altered by dissolution during the diffusion from LNAPL to groundwater (Thullner et al., 2013). Table 1 presents the $\partial^{13}C$ for ethylbenzene, m,p-xylenes and o-xylene in sampled LNAPL, showing an overall low variability in carbon isotope composition of less than one ‰. . Benzene and toluene concentrations were below the detection limit for isotope analysis and thus could not be used to evaluate the alteration of LNAPL.

Table 1 – Values of $\partial^{13}C$ for EX compounds in sampled LNAPL.

LNAPL Sample	Ethylbenzene (‰)	m/p-Xylenes (‰)	o-Xylene (‰)
RE-PM-94	bdl	-25.3 ± 0.2	-25.1 ± 0.5
RE-PM-98	bdl	-25.4 ± 0.2	-24.8 ± 0.7
RE-PM-95	-25.5 ± 0.3	-26.4 ± 0.1	-26.2 ± 0.1
RE-PM-53	-23.9 ± 0.5	-25.3 ± 0.1	-25.0 ± 0.2
RE-PM-98A	-25.3 ± 0.6	-25.2 ± 0.1	-24.8 ± 0.4
RE-PM-115A	-24.7 ± 0.6	-26.3 ± 0.1	-26.0 ± 0.2
RE-PM-100A	-25.8 ± 0.3	-26.4 ± 0.3	-25.8 ± 0.3
RE-PM-135	-26.6 ± 0.4	-26.6 ± 0.2	-25.9 ± 0.3
Average samples	-25.3 ± 0.5	-25.9 ± 0.2	-25.5 ± 0.3
Fresh jet fuel	-24.8 ± 0.7	-25.5 ± 0.1	-25.6 ± 0.2

*bdl = below the detection limit

The variability of the isotope composition of ethylbenzene and xylenes in the LNAPL was low and almost within the uncertainty of the analysis, demonstrating that the isotope signatures of ethylbenzene and xylenes in the

source were similar to those determined in the jet fuel (fresh kerosene from the refinery site). Thus, as expected, the LNAPL has conserved the isotope signature of the original jet fuel, and the isotope composition of ethylbenzene and xylenes within the phase have not been altered by chemical or biological processes overtime.

To improve our understanding of the dynamics of mass transfer in the source zone, we collected groundwater samples within the source zone during two sampling campaigns, in March 2015 and April 2016, as presented in Table 1 of the Supplementary Material. The obtained results of $\delta^{13}C$ of ethylbenzene in aqueous phase indicate that two of six samples in the first sampling campaign and eight of eleven samples in the second sampling campaign deviate noticeably with respect to the carbon isotopic signature of this compound in LNAPL (>2‰), demonstrating an enrichment of the compound by biodegradation. In the case of m,p-xylenes, one sample was significantly enriched in only the first sampling campaign, whereas the o-xylene showed significant deviation in one sample in the second sampling campaign (Figure 3). In the case of the first campaign, two of eight samples deviated more than 2‰ for ethylbenzene, three samples for m,p-xylenes, and none for o-xylenes. In the second campaign, seven of eleven samples deviated more than 2‰ for ethylbenzene. A lower enrichment of the isotope composition was observed for m,p-xylenes and o-xylenes. These results indicate specific trends of isotopic enrichment for the various compounds. In general, the results suggest that ethylbenzene, m,p-xylenes and o-xylene, show higher isotopic enrichment compared to these compounds in the LNAPL phase (Table 1), which clearly indicate degradation at high and low water table. Three samples—RE-PM-

115B, RE-PM-101B and RE-PM-81B—collected in the first and second sampling campaigns show a positive shift beyond 2‰ for m,p-xylenes. Downgradient of the LNAPL source zone, the plume of the dissolved phase is small to negligible because the high temperature provides conditions for fast mineralization of BTEX (Teramoto and Chang, 2019).

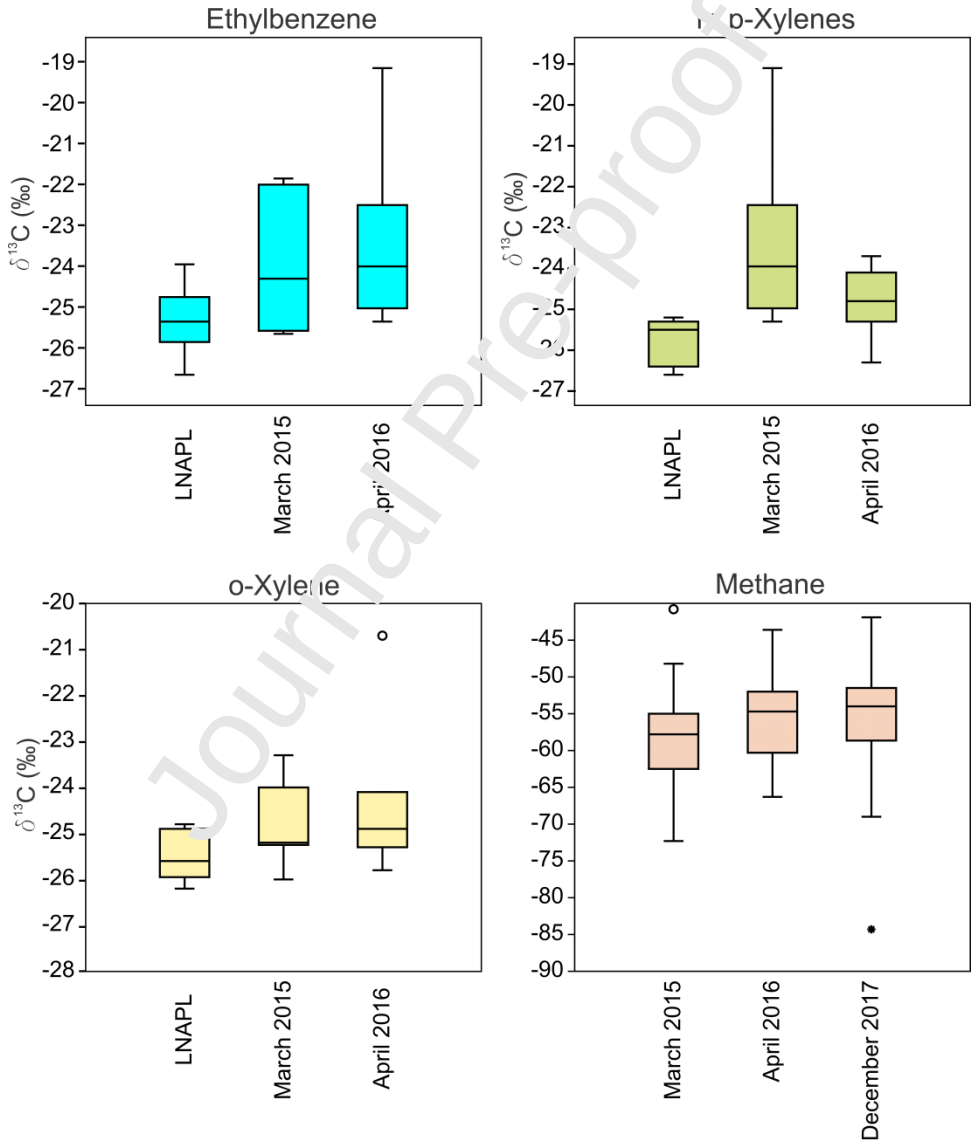

Figure 6 – Box plot of $\partial^{13}C$ for ethylbenzene, m,p-xylenes, o-xylenes in LNAPL, and for those dissolved in the aqueous phase in March 2015 and April 2016

samples. The box plot of $\partial^{13}C$ for methane in March 2015, April 2016 and December 2017 samples are also illustrated. The lower and upper limits of the box are the first and third quartiles, respectively, whereas the horizontal line inside the box represents the median.

The $\partial^{13}C$ of the isotopic signatures determined in LNAPL and groundwater samples collected in March 2015 and April 2016 were compared to quantify isotope enrichment (Figure 6). The medians of $\partial^{13}C$-BTEX in the aqueous phase are shifted to higher values, demonstrating the isotopic enrichment mediated by bacterial degradation. Likewise, the variances of measured $\partial^{13}C$-BTEX in the aqueous phase are higher than those measured in LNAPL. The increase of standard deviation of $\partial^{13}C$-BTEX in the aqueous phase may be associated with isotopic enrichment reflecting the extent of biodegradation. This parameter can be used as a criterion to diagnose the biodegradation within the LNAPL source zone.

3.3. Isotopes of CH_4 and CO_2

The evaluation of methane isotopic signature changes provides a complementary view of BTEX mineralization. The isotopic characterization of methane, conducted in April 2015, March 2016, and December 2017 are presented in Table 3 of the Supplementary Material. The determination of $\delta^{2}H$-CH_4 was possible in only 40 of the 89 collected samples in the three sampling campaigns because of low methane concentration in these groundwater

samples, particularly downgradient of the source zone. The range of ∂^{13}C-methane (Figure 6) varies in the three sampling campaigns, while the median possesses very low variation. The values of measured δ^2H and ∂^{13}C projected in diagram of Whiticar (1999) indicate that all samples fall within the field of bacterial production and most of them within the fermentation field, indicating that methanogenesis in the studied site is mainly acetoclastic.

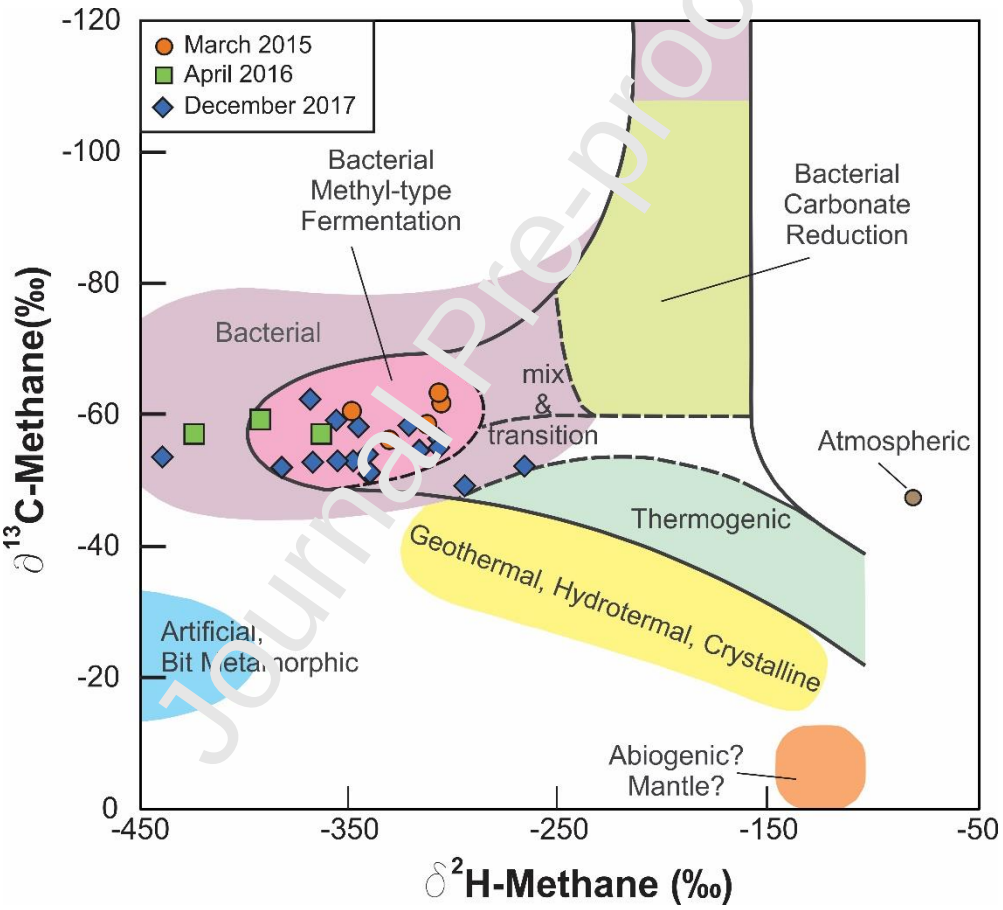

Figure 7 – Values of analyzed δ^2H and ∂^{13}C of methane, projected in diagram of Whiticar (1999) showing the delimited field of bacterial and thermogenic methane. Most of samples fall within the fermentation field.

The δ^2H-CH_4 is related to δ^2H-H_2O according empirical relationship described in Equation 2 (Whiticar, 1999).

$$\delta^2H - CH_4 = m(\delta^2H - H_2O) - \beta \quad (2)$$

Where m is equal to 1 in the case of carbonate reduction and 0.25 in the case of fermentation. The m parameter varies between -300 and -377 (Whiticar, 1999). The groundwater in the studied region have, respectively, δ^2H and δ^{18}O nearly -42 ‰ and -7‰ (Chang et al., 2020). Thus, the expected range of δ^2H-CH_4 varies between -310.5 and -387.5, typical of fermentative methanogenesis.

Most of samples fall within the isotope field of the fermentation (acetoclastic) when the values of ∂^{13}C-CO_2 and ∂^{13}C-CH_4 are projected in diagram presented by Milkov and Etiope (2018) (Figure 8), indicating that this mechanism represents the prevailing process associated with methane production.

Journal Pre-proof

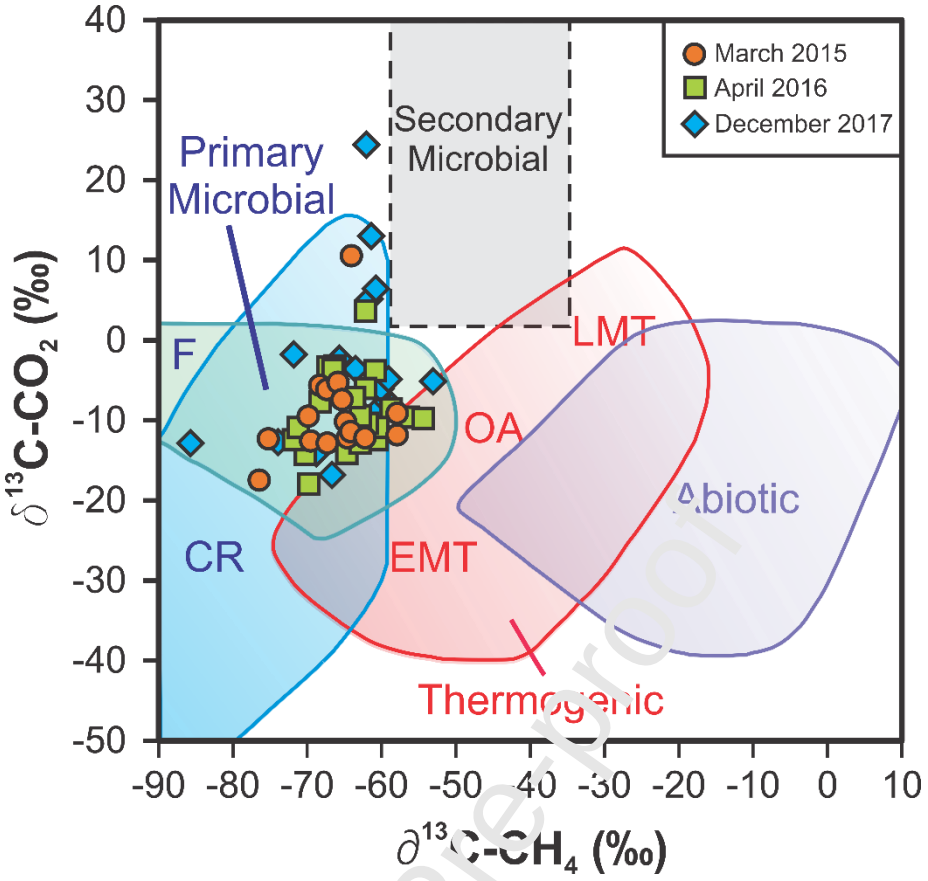

Figure 8 – Values of ∂^{13}C-CO$_2$ and ∂^{13}C-CH$_4$ projected in diagram presented by Milkov and Etiope (2018). Most of samples fall within the fermentative methanogenesis and are distributed along the oxidation trend.

Because of the reduced concentration, it was not possible to determine the δ^2H of methane in groundwater collected downgradient of LNAPL source zone, which hampered our interpretation. The ∂^{13}C-CH$_4$ values are, in general, more positive downgradient of the LNAPL source zone than inside it, suggesting an isotopic enrichment derived from methane oxidation along the flowlines. Notably, the map of ∂^{13}C-CO$_2$ displays a clear zoning with the enriched δ^{13}C-CO$_2$ values occupying the borders south and north of the LNAPL source zone and the more depleted values in the center (Figure 9).

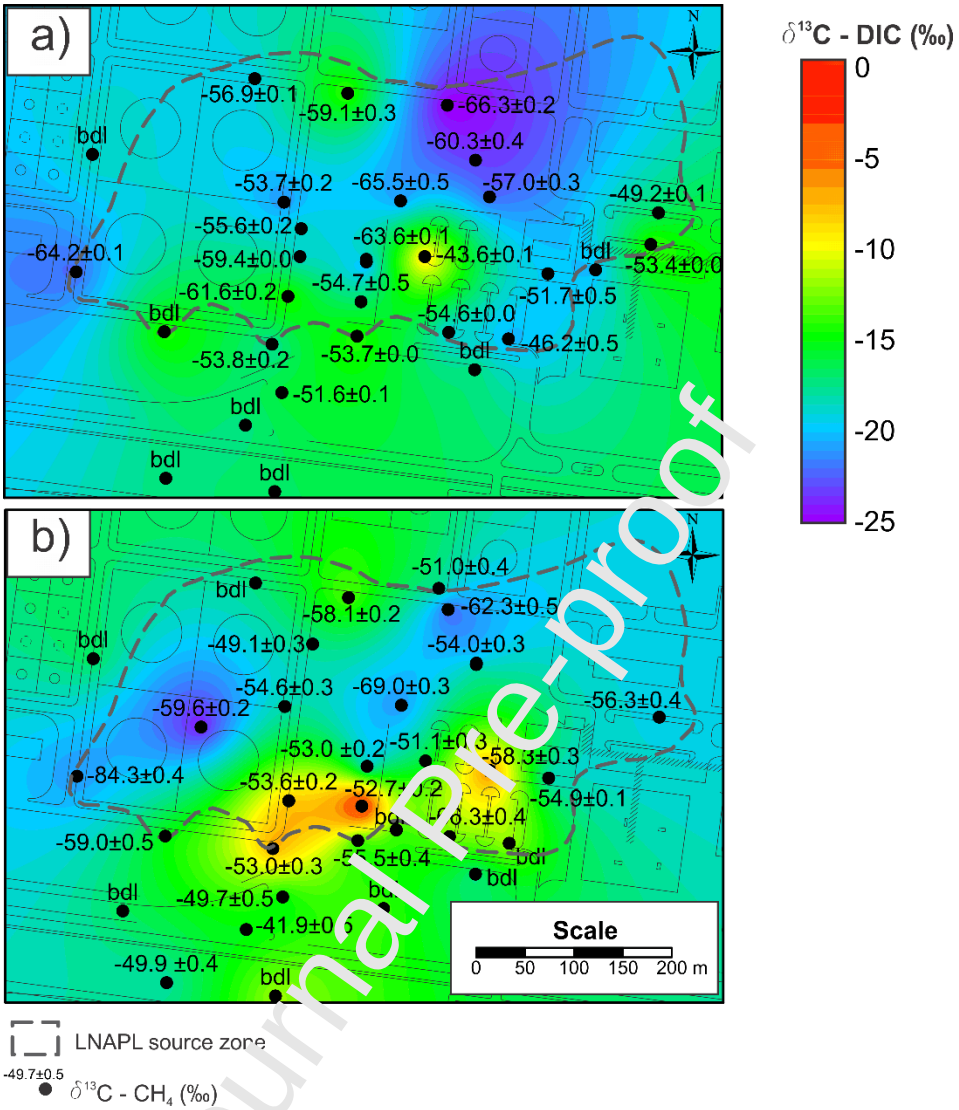

Figure 9 – Distribution of $\delta^{13}C$ values for methane compared to $\partial^{13}C$ for CO_2: a) April 2016, wet season; b) December 2017, dry season. Overall the CO_2 become lighter in wet season reflecting the release of CO_2 to groundwater possibly in the smear zone.

4. DISCUSSION

Journal Pre-proof

4.1. Isotope fractionation pattern of ethylbenzene, m,p-xylenes and o-xylenes

The mass transfer of LNAPLs to the aqueous phase is a complex phenomenon that is controlled by flow velocity, porosity, height of smear zone, and geometry of the bubble and ganglia of the entrapped LNAPL (Mobile et al., 2016; Saba & Illangasekare, 2000; Saenton & Illangasekare, 2007; Teramoto & Chang, 2017). The variation in biodegradation indicated by the $\partial^{13}C$ pattern of contaminants in the two sampling campaigns conducted in May 2015 and April 2016 (Figure 4) may therefore be attributed to the variation of flow rate and biodegradation kinetics. Hence, despite the continuous input of contaminants with the isotope composition of the source material during the interphase mass transfer from the LNAPs, our results showed a noticeable isotope enrichment of the compounds in aqueous phase compared to LNAPL. This suggests that the CSIA is able to validate the biodegradation within the water saturated zone close to the LNAPL source zone. The isotopic composition of BTEX in the aqueous phase varies with time and reflects the extent of biodegradation. The isotope composition of ethylbenzene and m-, p-xylene show a more prominent isotopic shift in May 2015 and a less extensive shift in April 2016, whereas o-xylene shows stronger enrichment in April 2016. These results indicate that the different compounds follow distinct temporal trends, reflecting differences in the mineralization or dissolution kinetics.

The low enrichment in some samples may also be related to aerobic biodegradation. These mechanisms were shown to be associated with rather small carbon isotope effects ($\varepsilon_C \leq 0.6‰$), while the anaerobic hydroxylation of the side chain of ethylbenzene by the enzyme ethylbenzene dehydrogenase is

characterized by noticeable carbon and hydrogen isotope effects ($\varepsilon_C \geq 3.7‰$). Monooxygenases acting on aromatics have been divided into four different types (Ullrich and Hofrichter, 2007); carbon isotope fractionation effects associated with monooxygenation of the aromatic ring were shown to range from low to considerable, probably due to the different reaction mechanisms of the different types of monooxygenases (Vogt et al., 2018).

4.2. Isotope pattern of of DIC and CH_4 in aqueous phase

The occurrence of anaerobic biodegradation of hydrocarbons driven mainly by iron reduction and methanogenesis was previously demonstrated by detection of a large plume of Fe(II) and methane (Teramoto and Chang, 2019). The isotopically “heavy” DIC in the border of LNAPL source zone (Figure 8) indicates the occurrence of anaerobic biodegradation (mainly due to methanogenesis). In contrast the similarity of ∂^{13}C-DIC to the average ∂^{13}C-BTEX value (~-25.5‰) for the LNAPL in the center of the source zone (Figure 6) strongly indicates aerobic biodegradation in this area. DIC progressively gets depleted in δ^{13}C downgradient of the southern edge of the source zone, most likely reflecting methane oxidation (Figure 8). This assumption challenged the intuitive conceptual model of methanogenic biodegradation prevalence in the center of the source zone and that of aerobic biodegradation at the edge. These results strongly suggest the dominance of the methanogenesis reaction along the north and south edges of the LNAPL source zone.

4.3. Development of a conceptual model

The seasonal fluctuating water table and air entrapment results in changing redox conditions in the smear zone (Teramoto and Chang, 2019). On this site, air entrapment is a seasonal and additional time varying driving force for biodegradation. The seasonal pattern is typically found in tropical areas with large seasonal precipitation patterns governing fluctuations of the water table. The isotopic data, presented in this work, in combination with microbiological data presented by Hidalgo et al. (2019) reinforces the importance of air entrapment and supports the reexamination of the conceptual model previously presented by Teramoto and Chang (2019). The main improvement over the previous geochemical conceptual model was the identification of an oxygenated region within the LNAPL source zone, created by air entrapment during water table rise. The new conceptual model is schematically illustrated in Figure 10.

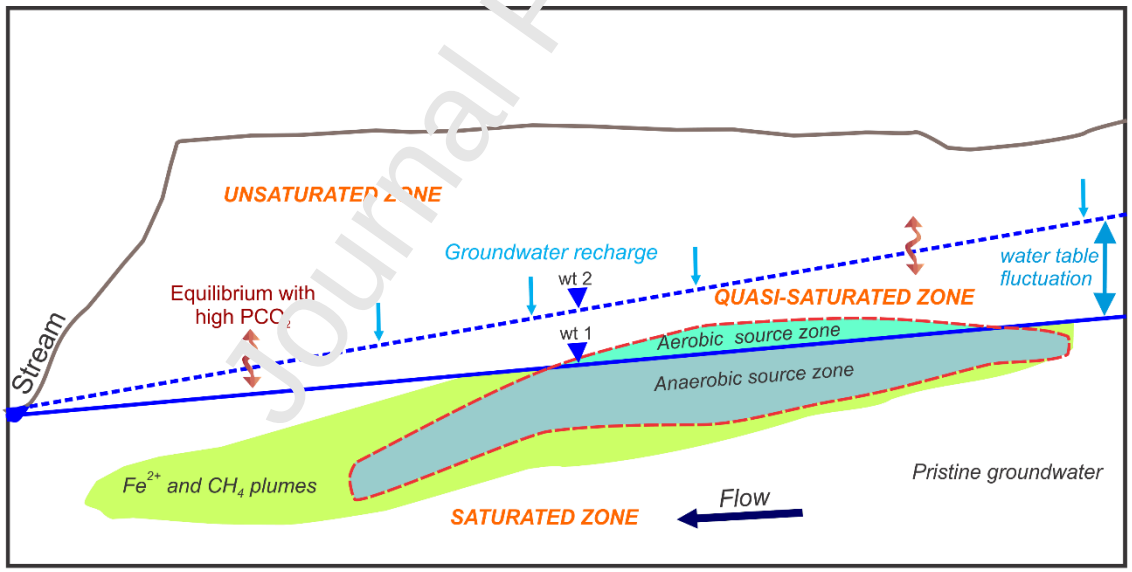

PRISTINE GROUNDWATER

Low mineralization in response to low residence time of groundwater and aquifer mineralogy simplicity, pH below 5 in responde to equilibrium with high PCO_2 (Teramoto & Chang, 2019).

SOURCE ZONE

Aerobic zone - the water table rise promotes the air entrapment and aquifer oxygenation. The oxygen is provided by diffusion of entrapped air. BTEX biodegradation is mediated by member of *Moraxellaceae* family (Hidalgo et al., 2019).

Anaerobic zone - anoxic zone, where the biodegradation is mainly mineralized by iron reduction and methanogenesis. The bacterial community is composed of *Propionibacteriaceae*, *Enterobacteriaceae*, *Geobacteriaceae* and *Peptococcaceae* (Hidalgo et al., 2019).. High concentration of Fe^{2+}, HCO_3^- and CH_4 associated to pH ranging from 5.5 to 6.2 (Teramoto & Chang, 2019).

Fe^{2+} AND CH_4 PLUMES

Mainly oxidant and very low BTEX concentration. Moderated to low concentration of Fe(II) and methane produced during the hydrocarbon biodegradation. pH and alkalinity higher than pristine groundwater

Figure 10 – Simplified cross-section of the conceptual model showing the distribution of biogeochemical zones, defined by geochemistry, microbiology and isotopic data.

4.3.1. Typical mineral phases and geochemistry of a pristine aquifer

The pristine groundwater displays low mineralization (electrical conductibility lower than 20 μS/cm), due to the reduced residence time and simplicity of aquifer mineralogy (Teramoto & Chang, 2019). The mineral phases that were identified in the studied aquifer were quartz (SiO_2), kaolinite ($Al_2Si_2O_5(OH)_4$), muscovite ($KAl_2(AlSi_3O_{10})(OH)_2$), and goethite ($FeO(OH)$); these are compatible with the lateritic nature of the studied aquifer. Because of the simplistic mineralogy and direct input of groundwater recharge, the electrical conductivity is usually greater than 20 μS/cm. The speciation calculation of the pristine groundwater buffered by a PCO_2 level of $10^{-1.5}$ atm, indicating a pH value of approximately 4.7 and an alkalinity value of less than 1 mg/L, which are similar to the field measurements.

4.3.2. LNAPL Source Zone

The analyses of 16S RNA, metagenomic, and isotopic analysis, indicate the stratification of the redox zone as well as the coexistence both aerobic and anaerobic zones within the LNAPL source zone (Figure 9). This finding is different from that in many field sites in temperate climates (e.g., Sutton et al., 2013; Fahrenfeld et al., 2014; Irianni-Reno et al., 2016), where microbes and

functional genes, strictly related to anaerobic biodegradation within the saturated zone containing LNAPL, were most abundant. The existence of an aerobic environment in the studied site is induced by fluctuation of the water table. During groundwater recharge, water invades the pores; both air and LNAPL are entrapped by capillary forces bellow the water table, creating a temporal zone with aerobic niches in the water saturated zone unless the oxygen from air entrapment is consumed. This oxygen is released in the water saturated zone by solubilization of entrapped air bubbles, which will form aerobic niches in an otherwise anoxic environment. This is explained by the abundance of aerobic and anaerobic microbes in the same zone stretching along the fluctuation of the water table.

The evaluation of the LIF transect (Figure 2), crossing the LNAPL source zone, reveals that LNAPL in the center of the source zone is distributed in the uppermost region of the saturated zone determined by water table fluctuation. On the other hand, in the areas of middle to southern edges of the source zone, LNAPL is strongly entrapped and smeared along the depth interval of water fluctuations and a major portion of LNAPL is located at the top of the water table. Thus, within the LNAPL source zone, there is a stratified environment, in which oxic and anoxic zones coexist. The direct evidence of oxygenation stratification was obtained by metagenomic and 16S rRNA investigations presented by Hidalgo et al. (2019). As demonstrated in this work, aerobic degraders of aliphatic and aromatic compounds *(*member of the *Moraxellaceae* family) revealed by metagenomic analysis, are found at the top of the saturated zone. The metagenomic analysis identified genes for benzoate degradation via catechol (*ben*ABCD) and encoded for catechol 1,2-dioxygenase (*cat*A); both

Journal Pre-proof

associated with the *Moraxellaceae* family were identified. Thus, the aerobic biodegradation in the center of the source zone, indicated by the measured ∂^{13}C-DIC, is related to the distribution of LNAPL within the aerobic zone (Figure 10). On the other hand, in the southern region of the source zone, LNAPL is mainly distributed below the oxygenated zone (Figure 10) and anaerobic biodegradation prevails. The values of ∂^{13}C-DIC in the southern source zone indicate anaerobic biodegradation and correspond with the high concentrations of CH_4 and Fe^{2+} observed in this region (Figure 3).

An anoxic environment prevails below the zone of bubble entrapment, with average pH and alkalinity of nearly 5.62 and 44.05 mg/L, respectively (Teramoto & Chang, 2019). The co-occurrence of iron-reduction and methanogenesis pathways indicate the existence of both hydrocarbon pathways, which lead to high concentration of Fe^{2+} and CH_4 within the LNAPL source zone (Figure 3). Several studies (e.g., Chapelle et al., 1992, Cozzarelli et al., 2001; Schreiber et al., 2004; Miles et al., 2008) have demonstrated that biodegradation under Fe(III) reduction and methanogenesis can occur in biogeochemical niches of the same zone showing compartmentation of the soil column. According to previous works (e.g., Siegert et al., 2011; Kato et al., 2012; Zhuang et al., 2015), the syntrophic metabolism related to methanogenesis is favored in presence of iron oxides. Under this condition, the abundance of iron oxide observed at the edge of LNAPL source zone favors the co-occurrence of iron-reduction and methanogenesis pathways. In some places where the iron was depleted by reductive reactions related to hydrocarbon biodegradation, methanogenesis dominates and the concentration of CH_4 is higher, while the concentration of Fe^{2+} is modest. As observed in Figure 3, in

the center of LNAPL source zone, the concentration of both CH_4 and Fe^{2+} are lower, suggesting the prevalence of aerobic biodegradation. The presence of oxygen at the aerobic zone inhibits the methanogenesis and the transition of aerobic to methanogenic zones is likely abrupt.

Although genes related to methanogenic have not been found via metagenomic analysis, Hidalgo et al. (2019) found genes related to the initial steps of methanogenesis as well as those involved in other general cell cycle reactions such as *hdr*B2 and *hdr*C2 encoding for heterodisulfide reductase enzyme complex. Hidalgo et al. (2019) also found *Propionibacteriaceae* and *Enterobacteriaceae* families at a depth of 1.2 m below the water table and *Geobacteriaceae* and *Peptococcaceae* familie colonizing in-situ microcosm installed 1.2 to 3.2 m bellow the water table. This finding supports the existence of anoxic environment bellow the oxygenated zone.

4.3.3. Fe^{2+} and CH_4 plume

A plume of Fe^{2+} and CH_4 stretches downgradient from the LNAPL source zone. This zone is generated by advective migration of Fe^{2+} and CH_4, produced by hydrocarbon biodegradation under iron and methanogenesis, respectively; these are transported with the water flow downgradient from the LNAPL source zone. The values of average pH, alkalinity, and electrical conductivity are significantly lower than those values observed in the LNAPL source zone.

The Fe^{2+} and CH_4 concentrations with alternating cycles of varying concentrations display an inverse trend with respect to fluctuation of the water table. Teramoto & Chang (2019) interpreted this variation as changes in redox

state of the aquifer due to the influx of oxygen during water table rise and consequent air entrapment in the uppermost portion of the saturated zone. However, this behavior may reflect a simple dilution during groundwater recharge when there is an input of clean water at the top of the saturated zone.

The $\partial^{13}C\text{-}CH_4$ and $\partial^{13}C$-DIC in the metabolic plume are similar to that in the southern region of the LNAPL source zone (Figure 8), suggesting that the methane oxidation contribution of light CO_2 is not very pronounced. On the contrary, enrichment of $\partial^{13}C\text{-}CH_4$ and fractionation of $\partial^{13}C$-DIC is only visible at the edge of the CH_4 plume. Because the LNAPL middle to southern edge of the source zone is distributed below the oxygenated zone, the produced CH_4 and Fe^{2+} plumes are also distributed below this zone (Figure 9). The low oxygenation content prevents the Fe^{2+} oxidation and maintains the $\partial^{13}C\text{-}CH_4$ and $\partial^{13}C$-DIC values as relatively stable over long distances from source zone.

5. CONCLUSIONS

The new insights provided by CSIA in the present study significantly enhance the previous findings at the study site with respect to the mechanism involved in the release and mineralization of hydrocarbons. Our results demonstrate that isotopic analysis of groundwater collected within the source zone can be applied to understand the overlap of mass transfer and biodegradation within the source zone. The isotope and geochemical parameters were used to characterize natural attenuation process of LNAPLs with an aquifer in tropical areas, lateritic soil columns and with typical large fluctuation of the water columns. The water table fluctuation, formation of a smear zone and entrapment of air lead to a compartmentation of the aquifer into

temporal geochemical niches disturbing a clear geochemical zonation according to the availability of electron acceptors and donators. The zones of aerobic, iron-reducing and methanogenic biodegradation were overlapping and indicating a strong spatial and temporal fluctuation correlated the precipitation pattern and rise and fall of the water table. The results of this study serve as an important reference for future research encompassing biodegradation of hydrocarbons in tropical climates.

ACKNOWLEDGEMENTS

We would like to acknowledge support from FUNDUNESP/UNESP, the Helmholtz Centre for Environmental Research–UFZ, Brazilian Petroleum Corporation–Petrobras –Petrobras, and the National Counsel for Technological and Scientific Development (CNPq) and the anonymous reviewers for critical suggestions used to improve the work.

REFERENCES

Aeppli, C., Berg, M., Cirpka, O. A., Holliger, C., Schwarzenbach, R. P., & Hofstetter, T. B. (2009). Influence of mass-transfer limitations on carbon isotope fractionation during microbial dechlorination of trichloroethene. *Environmental Science and Technology*, *43*(23), 8813–8820. https://doi.org/10.1021/es901481b

Alagappan, G.; Cowan, R. M. 2004. Effect of temperature and dissolved oxygen on the growth kinetics of Pseudomonas putida F1 growing on benzene and

toluene. *Chemosphere*, *54*(8), 1255-1265. Doi: https://10.1016/j.chemosphere.2003.09.013

Amos, R. T., Bekins, B. A., Delin, G. N., Cozzarelli, I. M., Blowes, D. W., & Kirshtein, J. D. (2011). Methane oxidation in a crude oil contaminated aquifer: Delineation of aerobic reactions at the plume fringes. *Journal of Contaminant Hydrology*, *125*(1–4), 13–25. https://doi.org/10.1016/j.jconhyd.2011.04.003

Balabane, M., Galimov, E., Hermann, M., & Létolle, R. (1987). Hydrogen and carbon isotope fractionation during experimental production of bacterial methane. *Organic Geochemistry*, *11*(2), 115–119. https://doi.org/10.1016/0146-6380(87)90033-7

Blum, P., Hunkeler, D., Weede, M., Beyer, C., Grathwohl, P., & Morasch, B. (2009). Quantification of biodegradation for o-xylene and naphthalene using first order decay models, Michaelis-Menten kinetics and stable carbon isotopes. *Journal of Contaminant Hydrology*, *105*(3–4), 118–130. https://doi.org/10.1016/j.jconhyd.2008.11.009

Bordignon, R., Teramoto, E. H., Chang, H. K., & Hespanhol, E. C. B. (2016). Caracterização isotópica de CO2 dissolvido em águas subterrâneas em área contaminada por querosene de aviação, município de Paulínia (SP). *Águas Subterrâneas*. https://doi.org/10.14295/ras.v29i3.27979

Bouchard, D.; Höhener, P.; Hunkeler, D. 2008. Carbon isotope fractionation during volatilization of petroleum hydrocarbons and diffusion across a porous medium: a column experiment. *Environmental Science & Technology*, *42*(21), 7801-7806. Doi: https://doi.org/10.1021/es800391s

Journal Pre-proof

Brook, G. A., Folkoff, M. E., Box, E. O. 1983. A world model of soil carbon dioxide. Earth Surface Processes and Landforms, 8(1), 79-88.

Chang, H. K., Gonçalves, R. D., Aggarwal, P. K., Stradioto, M. R., Hespanhol, E. C., Sturchio, N. C., ... & Araguas, L. J. (2020). Groundwater isotope ratios reflect convective and stratiform (paleo) precipitation fractions in Brazil. *Journal of Hydrology*, 124801. doi: https://doi.org/10.1016/j.jhydrol.2020.124801

Chapelle, F. H., & Lovley, D. R. 1992. Competitive exclusion of sulfate reduction by Fe (lll)-reducing bacteria: a mechanism for producing discrete zones of high-iron ground water. Ground Water, 30(1), 29-36. doi: 10.1111/j.1745-6584.1992.tb00808.x

Coleman, D. D., Risatti, J. B., & Schoell, M. (1981). Fractionation of carbon and hydrogen isotopes by methane-oxidizing bacteria. *Geochimica et Cosmochimica Acta*, *45*(7), 1033–1037. https://doi.org/10.1016/0016-7037(81)90129-0

Conrad, M. E., Daley, P. F., Fischer, M. L., Buchanan, B. B., Leighton, T., & Kashgarian, M. (1997). Combined 14C and δ13C monitoring of in situ biodegradation of petroleum hydrocarbons. *Environmental Science and Technology*, *31*(5), 1463–1469. https://doi.org/10.1021/es9607143

Coplen, T. B.; Brand, W. A.; Gehre, M.; Gröning, M. 2006. After two decades a second anchor for the VPDB delta13C scale. *Rapid Communications in Mass Spectrometry*, 20, 3565–3566. https://doi.org/10.1002/rcm

Coplen, T. B. 2011. Guidelines and recommended terms for expression of

stable-isotope-ratio and gas-ratio measurement results. *Rapid Communications in Mass Spectrometry*, *25*(17), 2538–2560. https://doi.org/10.1002/rcm.5129

Cozzarelli, I. M., Bekins, B. A., Baedecker, M. J., Aiken, G. R., Eganhouse, R. P., Tuccillo, M. E. 2001. Progression of natural attenuation processes at a crude-oil spill site: I. Geochemical evolution of the plume. Journal of Contaminant Hydrology, 53(3), 369-385. doi: 10.1016/S0169-7722(01)00174-7

Deeb, R. A.; Alvarez-Cohen, L. 1999. Temperature effects and substrate interactions during the aerobic biotransformation of BTEX mixtures by toluene-enriched consortia and Rhodococcus rhodochrous. *Biotechnology and Bioengineering*, *62*(5), 526-536. Doi: https://doi.org/10.1002/(SICI)1097-0290(19990305)62:5<526::AID-BIT4>3.0.CO;2-8

Dorer, C., Höhener, P., Hedwig, N., Richnow, H. H., & Vogt, C. (2014). Rayleigh-based concept to tackle strong hydrogen fractionation in dual isotope analysis - The example of ethylbenzene degradation by aromatoleum aromaticum. *Environmental Science and Technology*, *48*(10), 5788–5797. https://doi.org/10.1021/es404837g

Dorer, C., Vogt, C., Kleinsteuber, S., Stams, A. J. M., & Richnow, H. H. (2014). Compound-specific isotope analysis as a tool to characterize biodegradation of ethylbenzene. *Environmental Science and Technology*, *48*(16), 9122–9132. https://doi.org/10.1021/es500282t

Dorer, C., Vogt, C., Neu, T. R., Stryhanyuk, H., & Richnow, H. H. (2016). Characterization of toluene and ethylbenzene biodegradation under nitrate-,

iron(III)- and manganese(IV)-reducing conditions by compound-specific isotope analysis. *Environmental Pollution*, *211*(January), 271–281. https://doi.org/10.1016/j.envpol.2015.12.029

Durnford, D., Brookman, J., Billica, J., & Milligan, J. (1991). LNAPL distribution in a cohesionless soil: A field investigation and cryogenic sampler. *Groundwater Monitoring & Remediation*, 11(3), 115-122. Doi: https://doi.org/10.1111/j.1745-6592.1991.tb00387.x

Elsner, M., Zwank, L., Hunkeler, D., & Schwarzenbach, R. P. (2005). A new concept linking observable stable isotope fractionation to transformation pathways of organic pollutants. *Environmental Science and Technology*, *39*(18), 6896–6916. https://doi.org/10.1021/es0504587

EPA. (1996). U . S . ENVIRONMENTAL PROTECTION AGENCY REGION I LOW STRESS (low flow) PURGING AND SAMPLING PROCEDURE FOR THE COLLECTION OF FROM MONITORING. *Environmental Protection*, 0–4.

Fahrenfeld, N., Cozzarelli, I. M., Bailey, Z., Pruden, A. 2014. Insights into biodegradation through depth-resolved microbial community functional and structural profiling of a crude-oil contaminant plume. *Microbial ecology*, *68*(3), 453-462. Doi: https://doi.org/10.1007/s00248-014-0421-6

Faybishenko, B. A. 1995. Hydraulic Behavior of Quasi-Saturated Soils in the Presence of Entrapped Air: Laboratory Experiments. *Water Resources Research*, *31*(10), 2421–2435. https://doi.org/10.1029/95WR01654

Feisthauer, S., Seidel, M., Bombach, P., Traube, S., Knöller, K., Wange, M., …

Journal Pre-proof

Richnow, H. H. (2012). Characterization of the relationship between microbial degradation processes at a hydrocarbon contaminated site using isotopic methods. *Journal of Contaminant Hydrology*, *133*, 17–29. https://doi.org/10.1016/j.jconhyd.2012.03.001

Feisthauer, S., Vogt, C., Modrzynski, J., Szlenkier, M., Krüger, M., Siegert, M., & Richnow, H. H. (2011). Different types of methane monooxygenases produce similar carbon and hydrogen isotope fractionation patterns during methane oxidation. *Geochimica et Cosmochimica Acta*, *75*(5), 1173–1184. https://doi.org/10.1016/j.gca.2010.12.006

Fischer, A., Vieth, A., Knöller, K., Wachter, T., Dahmke, A., & Richnow, H. H. (2004). Charakterisierung des mikrobiellen Schadstoffabbaus mithilfe von isotopenchemischen Methoden. *Grundwasser*, *9*(3), 159–172. https://doi.org/10.1007/s00767-004-0042-y

Fry, V. A., Selker, J. S., & Gorelick, S. M. (1997). Experimental investigations for trapping oxygen gas in saturated porous media for in situ bioremediation. *Water Resources Research*, *33*(12), 2687–2696. https://doi.org/10.1029/97WR02428

Games, L.M.; Hayes, J.M.; Gunsalus, R. P. (1978). Methane-producing bacteria : natural fractionations of tbe stable carbon isotopes, *42*, 1295–1297.

Garg, S., Newell, C. J., Kulkarni, P. R., King, D. C., Adamson, D. T., Renno, M. I., & Sale, T. (2017). Overview of Natural Source Zone Depletion: Processes, Controlling Factors, and Composition Change. *Groundwater Monitoring and Remediation*, *37*(3), 62–81.

https://doi.org/10.1111/gwmr.12219

Gieg, L. M., Fowler, S. J., & Berdugo-Clavijo, C. (2014). Syntrophic biodegradation of hydrocarbon contaminants. *Current Opinion in Biotechnology*, *27*, 21–29. https://doi.org/10.1016/j.copbio.2013.09.002

Herrmann, S., Vogt, C., Fischer, A., Kuppardt, A., & Richnow, H. H. (2009). Characterization of anaerobic xylene biodegradation by two-dimensional isotope fractionation analysis. *Environmental Microbiology Reports*, *1*(6), 535–544. https://doi.org/10.1111/j.1758-2229.2009.00076.x

Heße, F., Prykhodko, V., Attinger, S., & Thullner, M. (2014). Assessment of the impact of pore-scale mass-transfer restrictions on microbially-induced stable-isotope fractionation. *Advances in Water Resources*, *74*, 79–90. https://doi.org/10.1016/j.advwatres.2014.08.007

Hidalgo, K. J., Teramoto, E. H., Soriano, A. U., Valoni, E., Baessa, M. P., Richnow, H. H., … Valeria, M. O. (2019). Taxonomic and functional diversity of the microbiome in a jet fuel contaminated site as revealed by combined application of in situ microcosms with metagenomic analysis. *Science of the Total Environment*, 135152. https://doi.org/10.1016/j.scitotenv.2019.135152

Holocher, J., Peeters, F., Aeschbach-Hertig, W., Hofer, M., Brennwald, M., Kinzelbach, W., & Kipfer, R. (2002). Experimental investigations on the formation of excess air in quasi-saturated porous media. Geochimica et Cosmochimica Acta, 66(23), 4103-4117. Doi: https://doi.org/10.1016/S0016-7037(02)00992-4

Journal Pre-proof

Irianni Renno, M., D. Akhbari, M.R. Olson, A.P. Byrne, E. Lefèvre, J. Zimbron, M. Lyverse, T.C. Sale, and S.K. De Long. 2016. Comparison of bacterial and archaeal communities in depth resolved zones in an LNAPL body. Applied Microbiology and Biotechnology 100, no. 7: 3347–3360. Doi: https://doi.org/10.1007/s00253-015-7106-z

Isler, E., Baessa, M. P. M., Teramoto, E. H., Pede, M. A. Z., & Kiang, C. H. (2018). Trapeamento de LNAPL observado por meio da técnica de fluorescência induzida por laser (LIF). *Águas Subterrâneas*. https://doi.org/10.14295/ras.v32i3.29137

Jiménez, N., Richnow, H., & Vogt, C. (2016). Methanogenic Hydrocarbon Degradation : Evidence from Field and Laboratory Studies, 227–242. https://doi.org/10.1159/000441679

Kato, S., Hashimoto, K., Watanabe, K. 2012. Methanogenesis facilitated by electric syntrophy via (semi) conductive iron-oxide minerals. Environmental microbiology, 14(7), 1646-1654. Doi: https://doi.org/10.1111/j.1462-2920.2011.02611.x

Kopinke F.D., Voskamp M., Georgi A., Richnow H.H. 2005. Carbon Isotope Fractionation of Organic Contaminants due to Retardation on Humic Substances – Implications for Natural Attenuation Studies in Aquifers. *Environ. Sci. Technol*., 39, 6052 - 6062. Doi: https://doi.org/10.1021/es040096n

Kopinke F. D., Georgi A., Imfeld G., Richnow H. H. (2017) Isotope fractionation of benzene during partitioning - Revisited. *Chemosphere* 168, 508–513. http://dx.doi.org/10.1016/j.chemosphere.2016.11.029

Journal Pre-proof

Lueders, T. (2017). The ecology of anaerobic degraders of BTEX hydrocarbons in aquifers. *FEMS Microbiology Ecology*, *93*(1), 1–13. https://doi.org/10.1093/femsec/fiw220

Mancini, S. A., Ulrich, A. C., Lacrampe-Couloume, G., Sleep, B., Edwards, E. A., & Lollar, B. S. (2003). Carbon and hydrogen isotopic fractionation during anaerobic biodegradation of benzene. *Applied and Environmental Microbiology*, *69*(1), 191–198. https://doi.org/10.1128/AEM.69.1.191-198.2003

Marinas, M., Roy, J. W., & Smith, J. E. (2013). Changes in entrapped gas content and hydraulic conductivity with pressure. *GroundWater*, *51*(1), 41–50. https://doi.org/10.1111/j.1745-6584.2012.00915.x

Mariotti, A., Germon, J. C., Hubert, P., Kaiser, P., Letolle, R., Tardieux, A., & Tardieux, P. (1981). Experimental determination of nitrogen kinetic isotope fractionation: Some principles, illustration for the denitrification and nitrification processes. *Plant and Soil*, *62*(3), 413–430. https://doi.org/10.1007/BF02374138

Mcleod, H. C., Roy, J. W., Smith, J. E. (2015). Patterns of entrapped air dissolution in a two-dimensional pilot-scale synthetic aquifer. *Groundwater*, *53*(2), 271–281. https://doi.org/10.1111/gwat.12203

Milkov, A. V., Etiope, G. (2018). Revised genetic diagrams for natural gases based on a global dataset of> 20,000 samples. *Organic Geochemistry*, *125*, 109-120. Doi: https://doi.org/10.1016/j.orggeochem.2018.09.002

Journal Pre-proof

Miles, B., Peter, A., Teutsch, G. 2008. Multicomponent simulations of contrasting redox environments at an LNAPL site. Ground Water, 46(5), 727-742. doi: https://doi.org/10.1111/j.1745-6584.2008.00457.x

Mobile, M., Widdowson, M., Stewart, L., Nyman, J., Deeb, R., Kavanaugh, M., … Gallagher, D. (2016). In-situ determination of field-scale NAPL mass transfer coefficients: Performance, simulation and analysis. *Journal of Contaminant Hydrology*, *187*, 31–46. https://doi.org/10.1016/j.jconhyd.2016.01.010

Morasch, B., Richnow, H. H., Schink, B., Vieth, A. & Meckenstock, R. U. (2002). Carbon and hydrogen stable isotope fractionation during aerobic bacterial degradation of aromatic hydrocarbons. *Applied and Environmental Microbiology*, *68*(10), 5191–5194. https://doi.org/10.1128/AEM.68.10.5191-5194.2002

Morris, B. E. L., Henneberger, R., Huber, H., & Moissl-Eichinger, C. (2013). Microbial syntrophy: interaction for the common good. *FEMS Microbiology Reviews*, *37*(3), 384–406. https://doi.org/10.1111/1574-6976.12019

Pede, M. A. Z. (2009). *Flutuação do lençol freático e sua implicação na recuperação de hidrocarbonetos: um estudo de caso*.

Ramos, D. T., da Silva, M. L. B., Nossa, C. W., Alvarez, P. J. J., & Corseuil, H. X. (2014). Assessment of microbial communities associated with fermentative-methanogenic biodegradation of aromatic hydrocarbons in groundwater contaminated with a biodiesel blend (B20). *Biodegradation*, *25*(5), 681–691. https://doi.org/10.1007/s10532-014-9691-4

Journal Pre-proof

Reinhard, M., Hopkins, G. D., Steinle-Darling, E., & LeBron, C. A. (2005). In situ biotransformation of BTEX compounds under methanogenic conditions. *Ground Water Monitoring and Remediation*, *25*(4), 50–59. https://doi.org/10.1111/j.1745-6592.2005.00046.x

Revesz, K., Coplen, T. B., Baedecker, M. J., Glynn, P. D., & Hult, M. (1995). Methane production and consumption monitored by stable H and C isotope ratios at a crude oil spill site, Bemidji, Minnesota. *Applied Geochemistry*, *10*(5), 505–516. https://doi.org/10.1016/0883-2927(95)00021-6

Richnow, H. H., Michaelis, W., Albrecht, P., Mahro, B., Seifert, R., Wehrung, P., & Eschenbach, A. (2002). The use of 13C-labelled polycyclic aromatic hydrocarbons for the analysis of their transformation in soil. *Chemosphere*, *36*(10), 2211–2224. https://doi.org/10.1016/s0045-6535(97)10193-x

Rolle, M.; Chiogna, G.; Bauer, R.; Griebler, C.; Grathwohl, P. 2010. Isotopic fractionation by transverse dispersion: Flow-through microcosms and reactive transport modeling study. *Environmental Science & Technology*, *44*(16), 6167-6173. Doi: https://doi.org/10.1021/es101179f

Saba, T., & Illangasekare, T. H. (2000). Effect of groundwater flow dimensionality on mass transfer from entrapped nonaqueous phase liquid contaminants. *Water Resources Research*, *36*(4), 971–979.

Saenton, S., & Illangasekare, T. H. (2007). Upscaling of mass transfer rate coefficient for the numerical simulation of dense nonaqueous phase liquid dissolution in heterogeneous aquifers. *Water Resources Research*, *43*(2), 1–15. https://doi.org/10.1029/2005WR004274

Journal Pre-proof

Schimmelmann, A., Qi, H., Coplen, T. B., Brand, W. A., Fong, J., Meier-Augenstein, W., … Werner, R. A. (2016). Organic Reference Materials for Hydrogen, Carbon, and Nitrogen Stable Isotope-Ratio Measurements: Caffeines, n-Alkanes, Fatty Acid Methyl Esters, Glycines, l -Valines, Polyethylenes, and Oils. *Analytical Chemistry*, *88*(8), 4294–4302. https://doi.org/10.1021/acs.analchem.5b04392

Schmidt, T. C., Zwank, L., Elsner, M., Berg, M., Meckenstock, R. U., & Haderlein, S. B. (2004). Compound-specific stable isotope analysis of organic contaminants in natural environments: A critical review of the state of the art, prospects, and future challenges. *Analytical and Bioanalytical Chemistry*, *378*(2), 283–300. https://doi.org/10.1007/s00216-003-2350-y

Schreiber, M. E., Carey, G. R., Feinstein, D. T., & Bahr, J. M. 2004. Mechanisms of electron acceptor utilization: implications for simulating anaerobic biodegradation. Journal of Contaminant Hydrology, 73(1), 99-127. doi: https://doi.org/10.1016/j.jconhyd.2004.01.004

Schüth, C.; Taubald, H.; Bolaño, N.; Maciejczyk, K. 2003. Carbon and hydrogen isotope effects during sorption of organic contaminants on carbonaceous materials. *Journal of Contaminant Hydrology*, *64*(3-4), 269-281. Doi: https://doi.org/10.1016/S0169-7722(02)00216-4

Siegert, M., Cichocka, D., Herrmann, S., Gründger, F., Feisthauer, S., Richnow, H. H., Krüger, M. (2011). Accelerated methanogenesis from aliphatic and aromatic hydrocarbons under iron-and sulfate-reducing conditions. FEMS microbiology letters, 315(1), 6-16. Doi: https://doi.org/10.1111/j.1574-6968.2010.02165.x

Journal Pre-proof

Steffy, D. A., Johnston, C. D., & Barry, D. A. (1998). Numerical simulations and long-column tests of LNAPL displacement and trapping by a fluctuating water table. *Journal of Soil Contamination*, 7(3), 325-356. Doi: https://doi.org/10.1080/10588339891334294

Sutton, N. B., Maphosa, F., Morillo, J. A., Al-Soud, W. A., Langenhoff, A. A., Grotenhuis, T., Smidt, H. 2013. Impact of long-term diesel contamination on soil microbial community structure. *Appl. Environ. Microbiol.*, *79*(2), 619-630. Doi: https://doi.org/10.1128/AEM.02747-12

Teramoto, E.H., & Chang, H. K. (2017). Field data and numerical simulation of btex concentration trends under water table fluctuations: Example of a jet fuel-contaminated site in Brazil. *Journal of Contaminant Hydrology*, *198*. https://doi.org/10.1016/j.jconhyd.2017.01.002

Teramoto, E.H., & Chang, H. K. (2019). Geochemical conceptual model of BTEX biodegradation in an iron-rich aquifer. *Applied Geochemistry*, *100*. https://doi.org/10.1016/j.apgeochem.2018.11.019

Teramoto, Elias Hideo, & Chang, H. K. (2017). Field data and numerical simulation of btex concentration trends under water table fluctuations: Example of a jet fuel-contaminated site in Brazil. *Journal of Contaminant Hydrology*, *198*, 37–47. https://doi.org/10.1016/j.jconhyd.2017.01.002

Teramoto, E. H., Chang, H. K. 2018. Métodos WTF e simulação numérica de fluxo para estimativa de recarga–exemplo Aquífero Rio Claro em Paulínia/SP. *Águas Subterrâneas*, *32*(2), 173-180. Doi: https://doi.org/10.14295/ras.v32i2.28943

Journal Pre-proof

Teramoto, Elias Hideo, & Chang, H. K. (2019). Geochemical conceptual model of BTEX biodegradation in an iron-rich aquifer. *Applied Geochemistry*, *100*(November 2018), 293–304. https://doi.org/10.1016/j.apgeochem.2018.11.019

Thullner, M., Fischer, A., Richnow, H. H., & Wick, L. Y. (2013). Influence of mass transfer on stable isotope fractionation. *Applied Microbiology and Biotechnology*, *97*(2), 441–452. https://doi.org/10.1007/s00253-012-4537-7

Ullrich, R., & Hofrichter, M. (2007). Enzymatic hydroxylation of aromatic compounds. *Cellular and Molecular Life Sciences*, *64*(3), 271–293. https://doi.org/10.1007/s00018-007-6362-1

Vogt, C., Cyrus, E., Herklotz, I., Schlosser, D., Bahr, A., Herrmann, S., … Fischer, A. (2008). Evaluation of toluene degradation pathways by two-dimensional stable isotope fractionation. *Environmental Science and Technology*, *42*(21), 7791–7800. https://doi.org/10.1021/es8003415

Vogt, C., Dorer, C., Musat, F., & Richnow, H. H. (2016). Multi-element isotope fractionation concepts to characterize the biodegradation of hydrocarbons - from enzymes to the environment. *Current Opinion in Biotechnology*, *41*, 90–98. https://doi.org/10.1016/j.copbio.2016.04.027

Vogt C., Musat F., Richnow H. H. (2018) Compound-Specific Isotope Analysis for Studying the Biological Degradation of Hydrocarbons. In: Boll M. (eds) Anaerobic Utilization of Hydrocarbons, Oils, and Lipids. Handbook of Hydrocarbon and Lipid Microbiology. Springer International Publishing.

Wang, D. T., Welander, P. V., & Ono, S. (2016). Fractionation of the methane

Journal Pre-proof

isotopologues 13 CH 4 , 12 CH 3 D, and 13 CH 3 D during aerobic oxidation of methane by Methylococcus capsulatus (Bath). *Geochimica et Cosmochimica Acta*, *192*, 186–202. https://doi.org/10.1016/j.gca.2016.07.031

Whiticar, M. J. (1999). Carbon and hydrogen isotope systematics of bacterial formation and oxidation of methane. *Chemical Geology*, *161*(1), 291–314. https://doi.org/10.1016/S0009-2541(99)00092-3

Whiticar, M. J., & Faber, E. (1986). Methane oxidation in sediment and water column environments-Isotope evidence. *Organic Geochemistry*, *10*(4–6), 759–768. https://doi.org/10.1016/S0146-6380(86)80013-4

Williams, M. D., & Oostrom, M. (2000). Oxygenation of anoxic water in a fluctuating water table system. An experimental and numerical study. *Journal of Hydrology*, *230*(1–2), 70–85. https://doi.org/10.1016/S0022-1694(00)00172-4

Yadav, B. K., Shrestha, S. R., & Hassanizadeh, S. M. (2012). Biodegradation of toluene under seasonal and diurnal fluctuations of soil-water temperature. *Water, Air, & Soil Pollution*, *223*(7), 3579-3588. Doi: https://doi.org/10.1007/s11270-011-1052-x

Zeman, N. R.; Renno, M. I.; Olson, M. R.; Wilson, L. P., Sale, T. C.; Susan, K. 2014. Temperature impacts on anaerobic biotransformation of LNAPL and concurrent shifts in microbial community structure. *Biodegradation*, *25*(4), 569-585. Doi: https://doi.org/10.1007/s10532-014-9682-5

Zengler K., Richnow H.H., Rossello-Mora R., Michaelis W., Widdel F. 1999. Methane formation from long-chain alkanes by anaerobic microorganisms. *Nature* 401, 266-269. Doi: https://doi.org/10.1038/45777

Journal Pre-proof

Zhuang, L., Tang, J., Wang, Y., Hu, M., Zhou, S. 2015. Conductive iron oxide minerals accelerate syntrophic cooperation in methanogenic benzoate degradation. Journal of hazardous materials, 293, 37-45. Doi: https://doi.org/10.1111/j.1574-6968.2010.02165.x

Journal Pre-proof

Credit author statement

Elias Hideo Teramoto: Conceptualization, Investigation, Formal analysis, Visualization, Writing- Original draft preparation, Writing – Review & Editing. **Carsten Vogt**: Methodology, Formal analysis, Writing – Original draft preparation, Writing – Review & Editing. **Marcus Paulus Martins Baessa**: Investigation. **Luciana Polese:** investigation. **Adriana Ururahy Soriano:** investigation. **Chang Hung Kiang:** Conceptualization**,** Supervision, Writing- Original draft preparation, Writing – Review & Editing. **Hans Richnow**: Formal analysis, Writing – Original draft preparation, Writing – Review & Editing.

Journal Pre-proof

The authors declare there is no conflict of interest whatsoever.

On behalf of the authors,

H. K. Chang

Journal Pre-proof

- $\partial\ ^{13}C$ of BTEX can provide valuable information regarding biodegradation within LNAPL source zone
- CH_4 produced by hydrocarbon biodegradation is mainly derived from fermentative methanogenesis
- $\delta^{13}C\text{-}CO_2$ values reveal that methanogenesis prevails at the border and aerobic biodegradation prevails in the center of LNAPL source zone

Journal Pre-proof

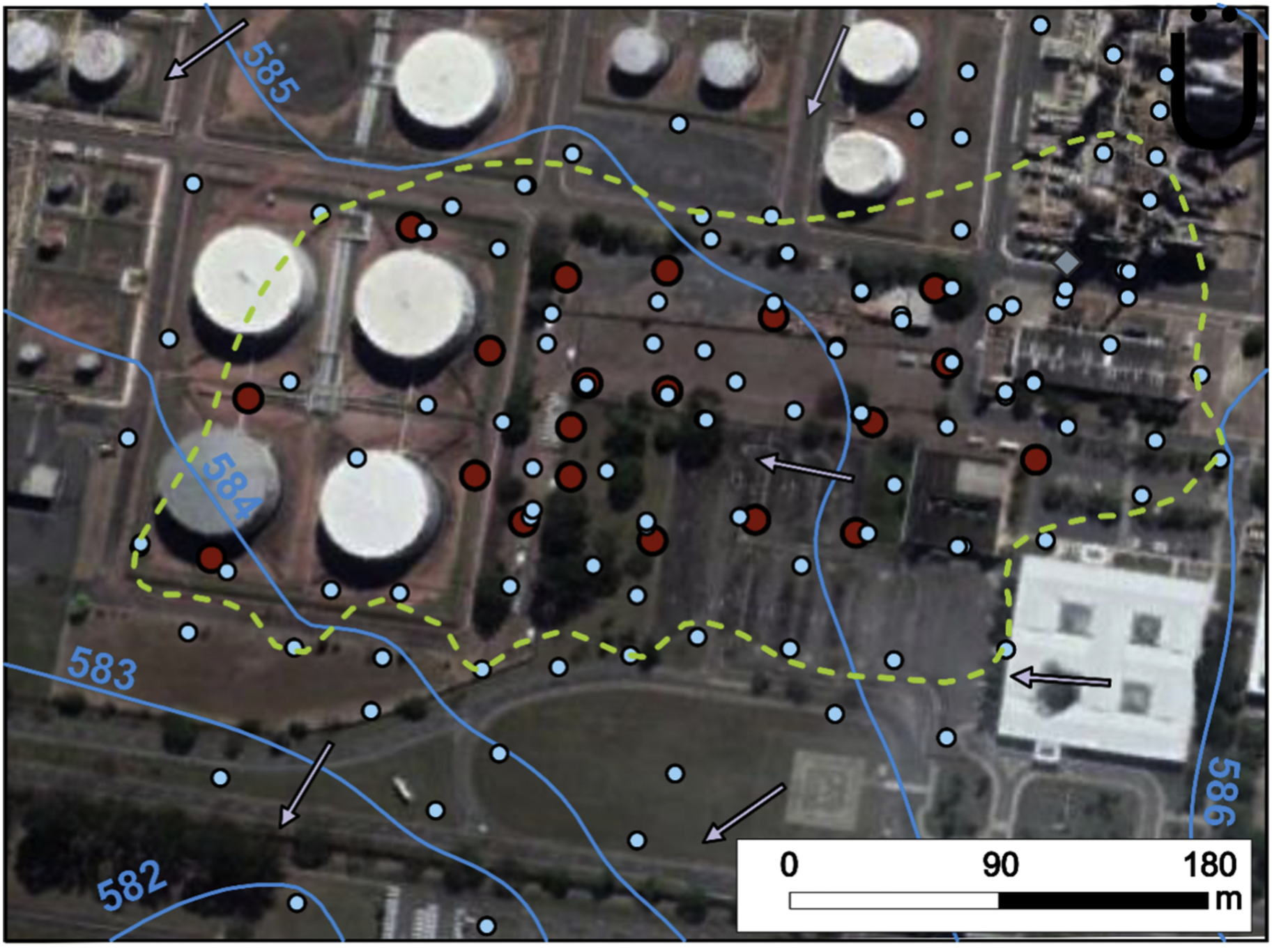

Legend

- Limir of LNAPL Source-zone
- Equipotential lines (m)
- Flow direction
- Leaking point
- Pumping wells
- Monitoring wells

Figure 1

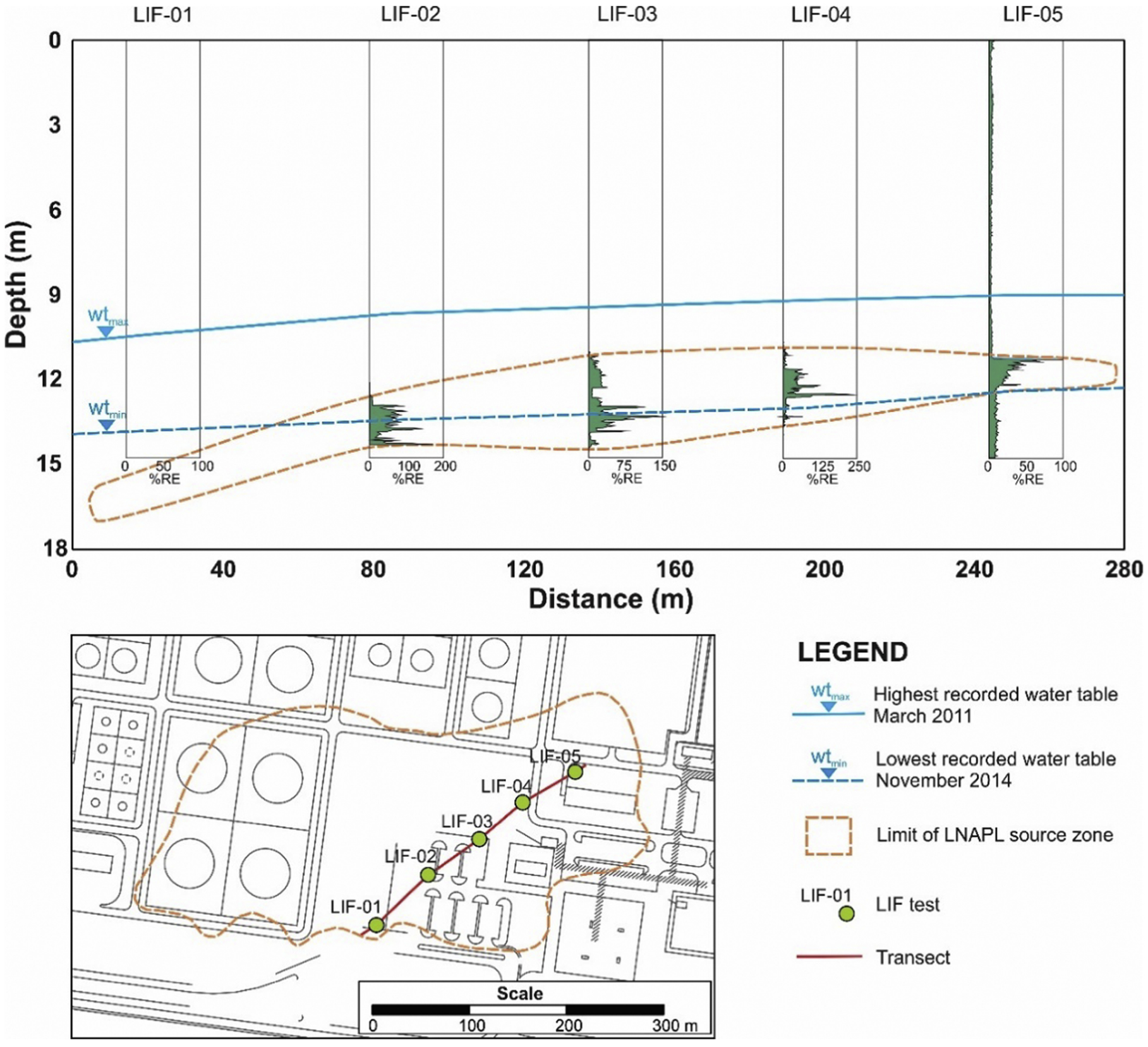
LIF-01
LIF-02
LIF-03
LIF-04
LIF-05
Depth (m)
0
3
6
9
12
15
18
wt_max
wt_min
0 50 100
%RE
0 100 200
%RE
0 75 150
%RE
0 125 250
%RE
0 50 100
%RE
0
40
80
120
160
200
240
280
Distance (m)
LIF-05
LIF-04
LIF-03
LIF-02
LIF-01
Scale
0 100 200 300 m
LEGEND
wt_max
Highest recorded water table
March 2011
wt_min
Lowest recorded water table
November 2014
Limit of LNAPL source zone
LIF-01
LIF test
Transect

Figure 2

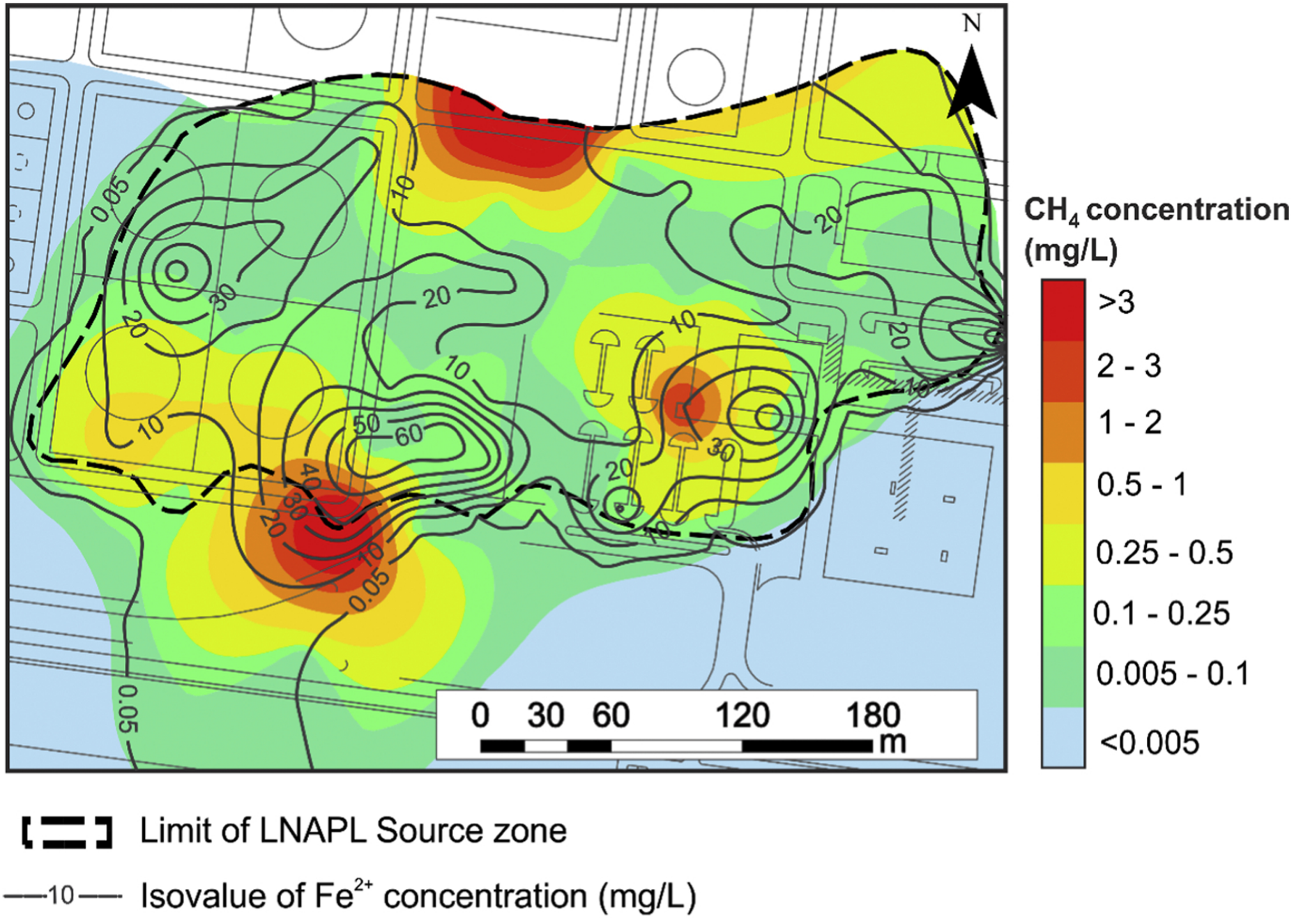
N
CH_4 concentration (mg/L)
>3
2 - 3
1 - 2
0.5 - 1
0.25 - 0.5
0.1 - 0.25
0.005 - 0.1
<0.005
0 30 60 120 180
m
Limit of LNAPL Source zone
10
Isovalue of Fe^{2+} concentration (mg/L)

Figure 3

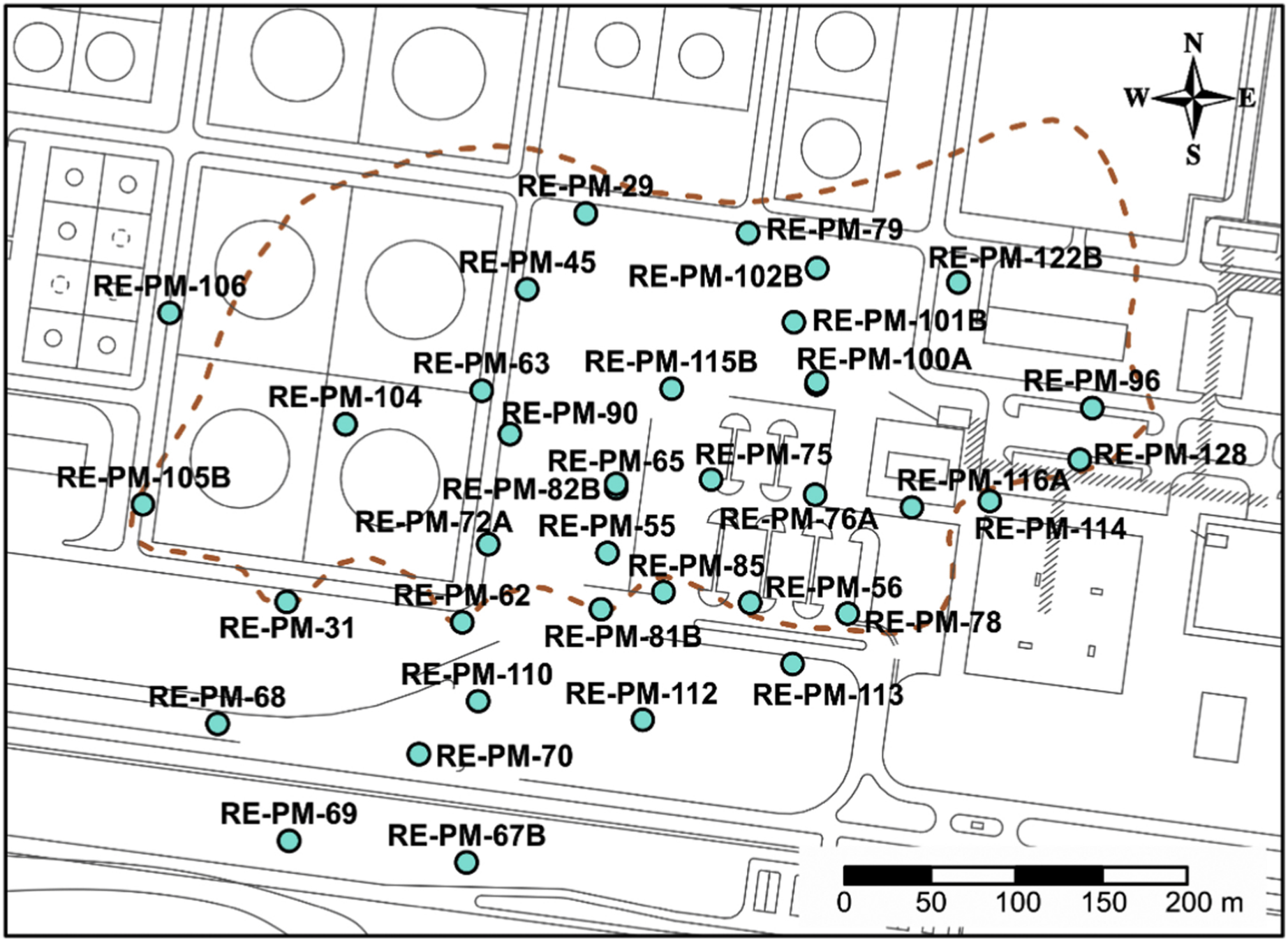
N
W
E
S
RE-PM-29
RE-PM-79
RE-PM-45
RE-PM-102B
RE-PM-122B
RE-PM-106
RE-PM-101B
RE-PM-63
RE-PM-115B
RE-PM-100A
RE-PM-96
RE-PM-104
RE-PM-90
RE-PM-65
RE-PM-75
RE-PM-128
RE-PM-105B
RE-PM-82B
RE-PM-116A
RE-PM-72A
RE-PM-55
RE-PM-76A
RE-PM-114
RE-PM-85
RE-PM-62
RE-PM-56
RE-PM-31
RE-PM-78
RE-PM-81B
RE-PM-110
RE-PM-68
RE-PM-112
RE-PM-113
RE-PM-70
RE-PM-69
RE-PM-67B
0
50
100
150
200 m
Limit of source zone
Sampled monitoring wells

Figure 4

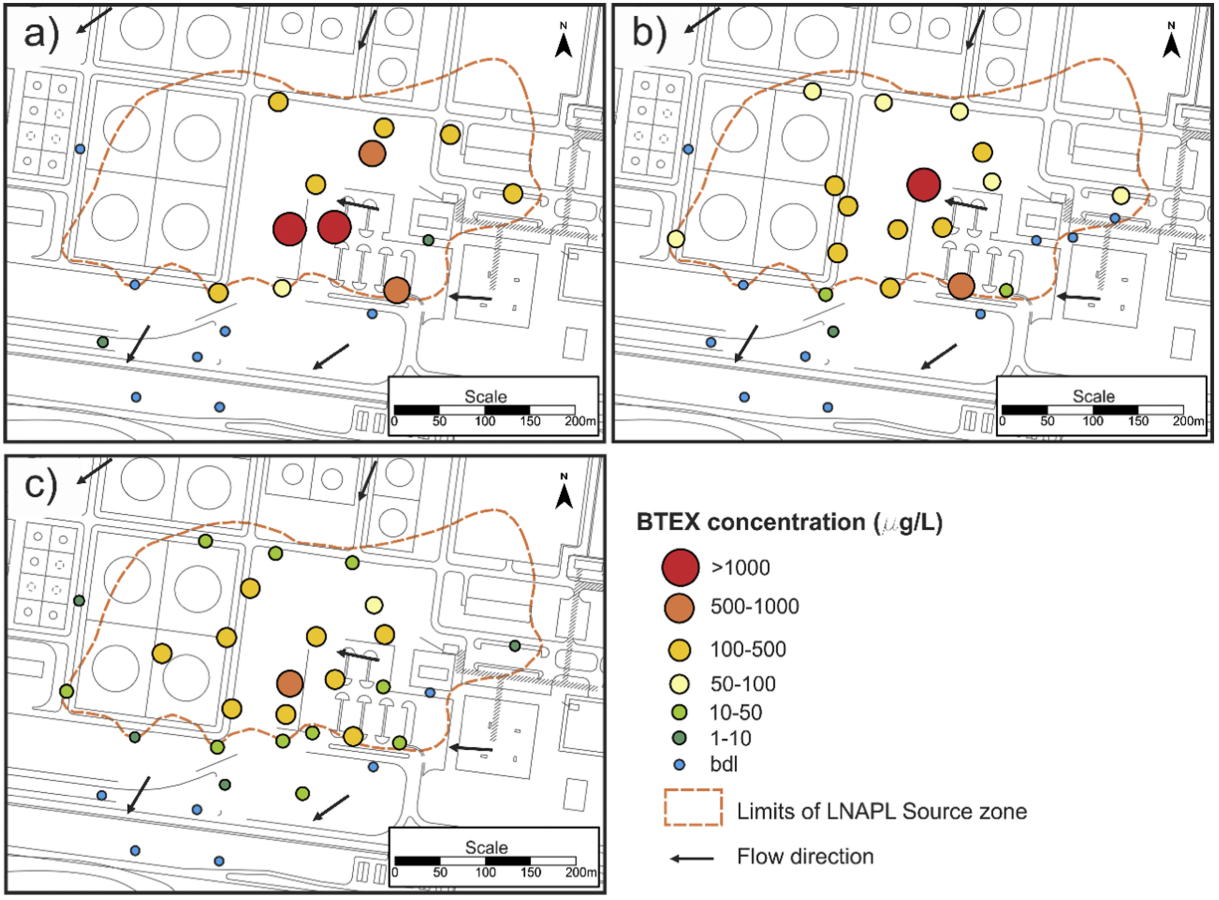
a)
b)
c)
N
Scale
0 50 100 150 200m
BTEX concentration (μg/L)
>1000
500-1000
100-500
50-100
10-50
1-10
bdl
Limits of LNAPL Source zone
Flow direction

Figure 5

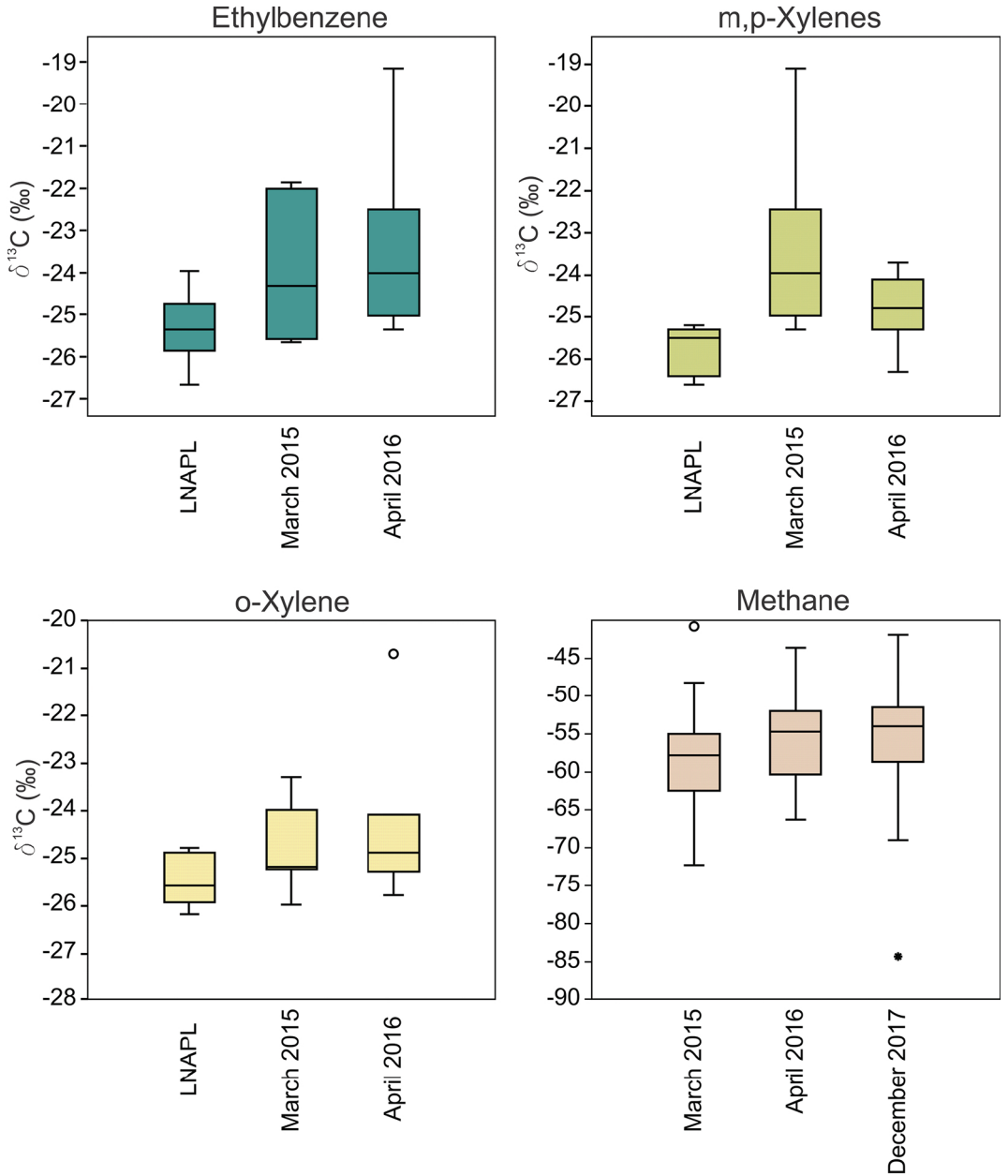
Ethylbenzene
m,p-Xylenes
o-Xylene
Methane
δ13C (‰)
LNAPL
March 2015
April 2016
December 2017

Figure 6

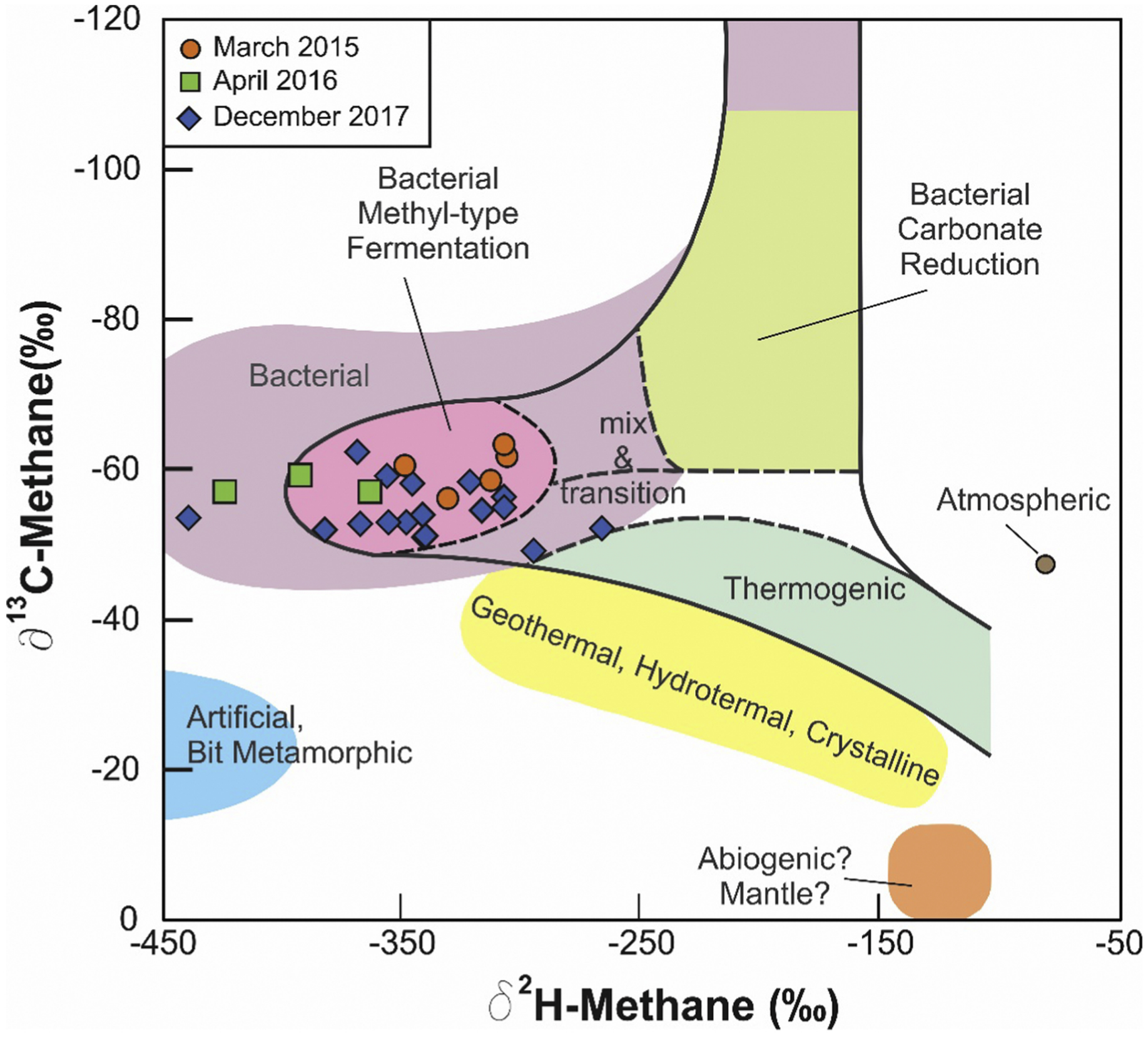
March 2015
April 2016
December 2017
Bacterial
Methyl-type
Fermentation
Bacterial
Carbonate
Reduction
Bacterial
mix
&
transition
Atmospheric
Thermogenic
Geothermal, Hydrotermal, Crystalline
Artificial,
Bit Metamorphic
Abiogenic?
Mantle?
-120
-100
-80
-60
-40
-20
0
-450
-350
-250
-150
-50
δ13C-Methane(‰)
δ2H-Methane (‰)

Figure 7

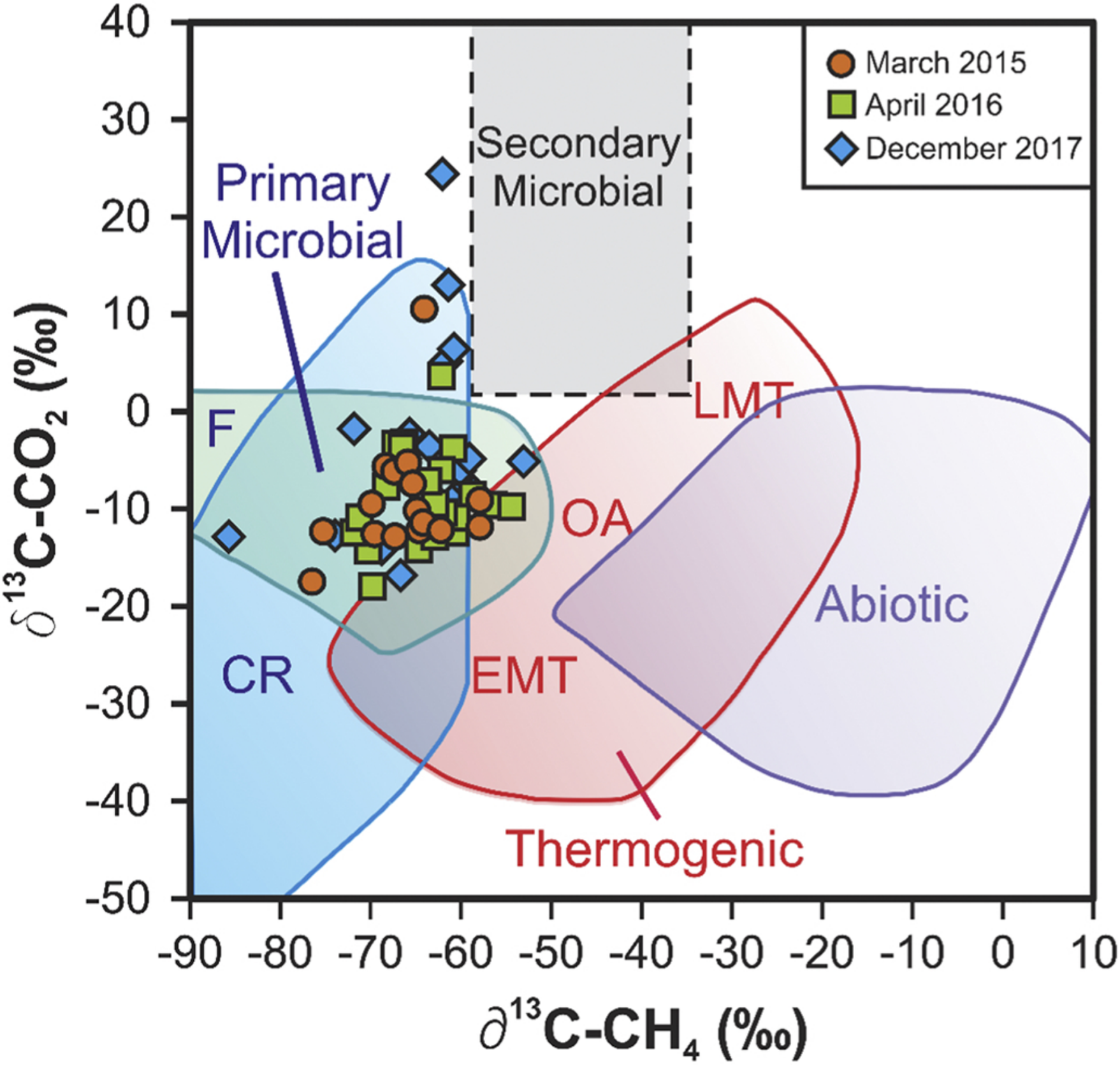
March 2015
April 2016
December 2017
Secondary Microbial
Primary Microbial
F
CR
LMT
OA
EMT
Abiotic
Thermogenic
40
30
20
10
0
-10
-20
-30
-40
-50
-90
-80
-70
-60
-50
-40
-30
-20
-10
0
10
δ^{13}C-CO$_2$ (‰)
∂^{13}C-CH$_4$ (‰)

Figure 8

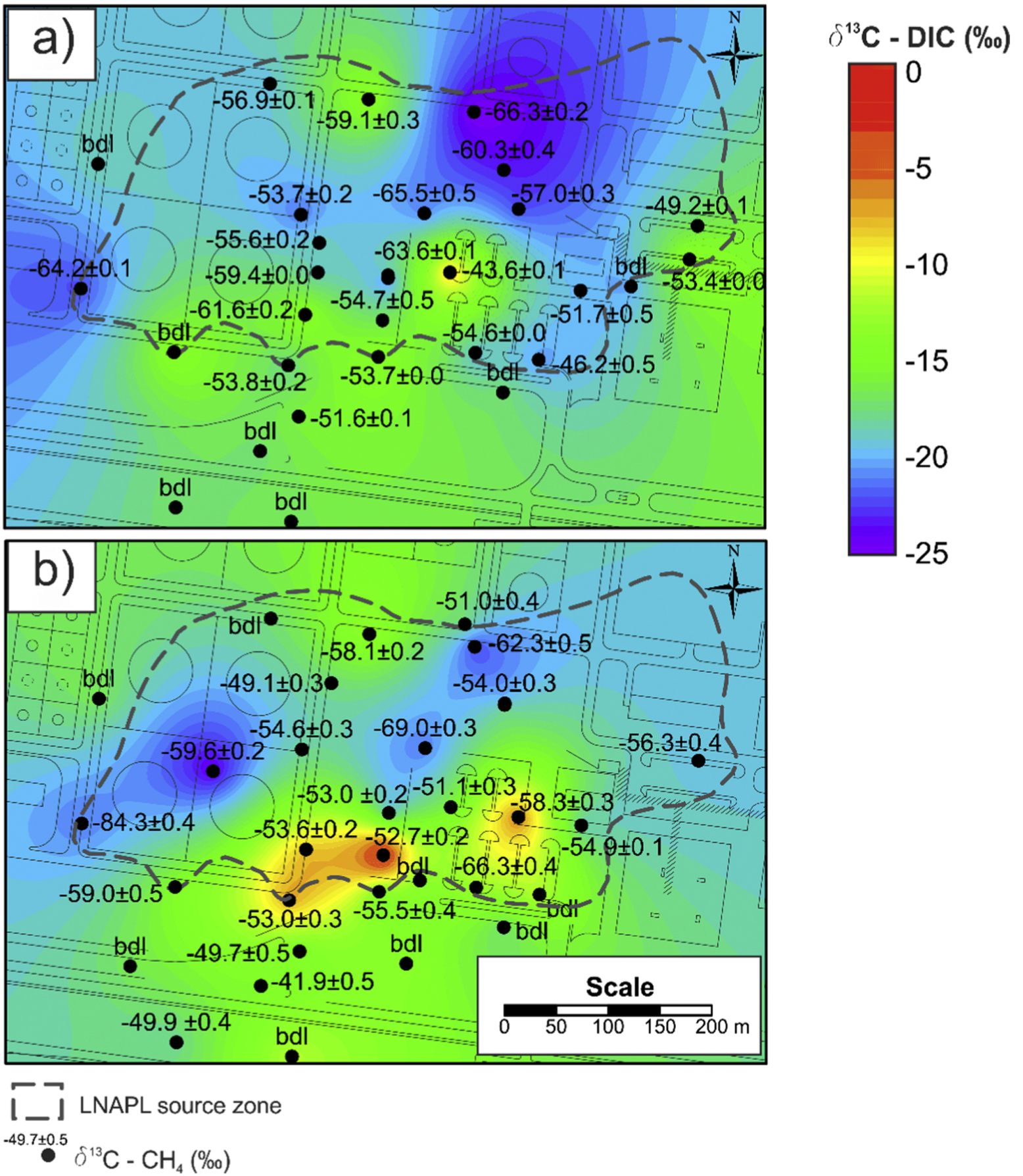
a)
b)
N
δ13C - DIC (‰)
0
-5
-10
-15
-20
-25
-56.9±0.1
-59.1±0.3
-66.3±0.2
bdl
-60.3±0.4
-53.7±0.2
-65.5±0.5
-57.0±0.3
-49.2±0.1
-55.6±0.2
-63.6±0.1
-64.2±0.1
-59.4±0.0
-43.6±0.1
bdl
-53.4±0.0
-61.6±0.2
-54.7±0.5
-51.7±0.5
bdl
-54.6±0.0
-46.2±0.5
-53.8±0.2
-53.7±0.0
bdl
-51.6±0.1
bdl
bdl
bdl
-51.0±0.4
bdl
-58.1±0.2
-62.3±0.5
bdl
-49.1±0.3
-54.0±0.3
-54.6±0.3
-69.0±0.3
-56.3±0.4
-59.6±0.2
-53.0 ±0.2
-51.1±0.3
-58.3±0.3
-84.3±0.4
-53.6±0.2
-52.7±0.2
-54.9±0.1
bdl
-66.3±0.4
-59.0±0.5
-53.0±0.3
-55.5±0.4
bdl
bdl
bdl
bdl
-49.7±0.5
-41.9±0.5
-49.9 ±0.4
bdl
Scale
0 50 100 150 200 m
LNAPL source zone
-49.7±0.5
δ13C - CH4 (‰)

Figure 9

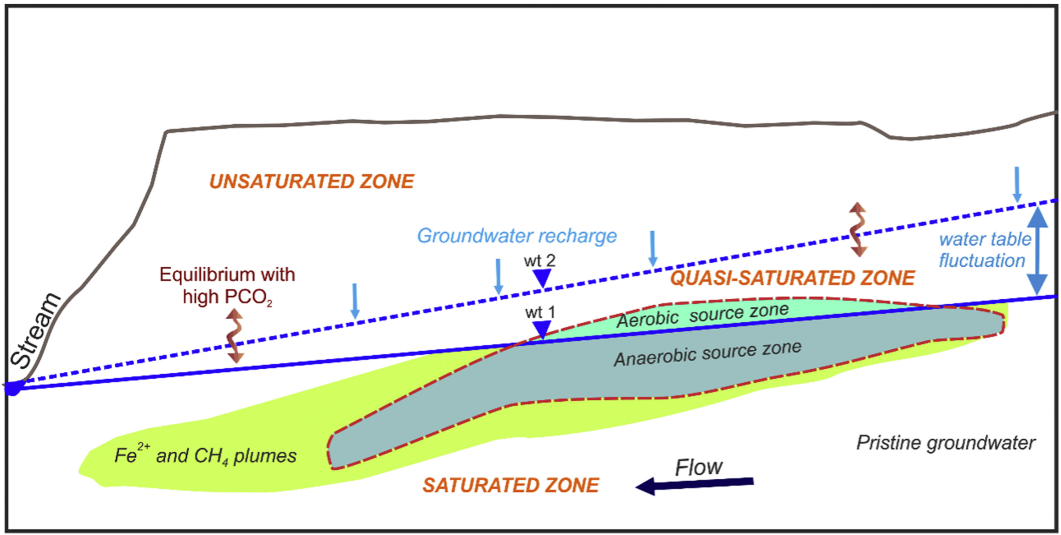

PRISTINE GROUNDWATER

Low mineralization in response to low residence time of groundwater and aquifer mineralogy simplicity, pH below 5 in responde to equilibrium with high PCO_2 (Teramoto & Chang, 2019).

SOURCE ZONE

Aerobic zone - the water table rise promotes the air entrapment and aquifer oxygenation. The oxygen is provided by diffusion of entrapped air. BTEX biodegradation is mediated by member of *Moraxellaceae* family (Hidalgo et al., 2019).

Anaerobic zone - anoxic zone, where the biodegradation is mainly mineralized by iron reduction and methanogenesis. The bacterial community is composed of *Propionibacteriaceae*, *Enterobacteriaceae, Geobacteriaceae* and *Peptococcaceae* (Hidalgo et al., 2019).. High concentration of Fe^{2+}, HCO_3^- and CH_4 associated to pH ranging from 5.5 to 6.2 (Teramoto & Chang, 2019).

Fe^{2+} AND CH_4 PLUMES

Mainly oxidant and very low BTEX concentration. Moderated to low concentration of Fe(II) and methane produced during the hydrocarbon biodegradation. pH and alkalinity higher than pristine groundwater

Figure 10